Homogeneous nucleation rate of methane hydrate formation under experimental conditions from seeding simulations

J. Grabowska ; S. Blazquez ; E. Sanz ; E. G. Noya ; I. M. Zeron ; J. Algaba ; J. M. Miguez ;
F. J. Blas ; C. Vega ✉

Check for updates

View Online   Export Citation   CrossMark

Homogeneous nucleation rate of methane hydrate formation under experimental conditions from seeding simulations (EP)

View Online   Export Citation   CrossMark

J. Grabowska,[1,2] (iD) S. Blazquez,[1] (iD) E. Sanz,[1] (iD) E. G. Noya,[3] (iD) I. M. Zeron,[4] (iD) J. Algaba,[4] (iD) J. M. Miguez,[4] (iD)
F. J. Blas,[4] (iD) and C. Vega[1,a)] (iD)

AFFILIATIONS

[1] Dpto. Química Física I, Fac. Ciencias Químicas, Universidad Complutense de Madrid, 28040 Madrid, Spain
[2] Department of Physical Chemistry, Faculty of Chemistry and BioTechMed Center, Gdansk University of Technology,
  ul. Narutowicza 11/12, 80-233 Gdansk, Poland
[3] Instituto de Química Física Rocasolano, CSIC, C/ Serrano 119, 28006 Madrid, Spain
[4] Laboratorio de Simulación Molecular y Química Computacional, CIQSO-Centro de Investigación en Química Sostenible and
  Departamento de Ciencias Integradas, Universidad de Huelva, 21006 Huelva, Spain

Note: This paper is part of the JCP Special Topic on Nucleation: Current Understanding Approaching 150 Years After Gibbs.
[a)] Author to whom correspondence should be addressed: cvega@quim.ucm.es

ABSTRACT

In this work, we shall estimate via computer simulations the homogeneous nucleation rate for the methane hydrate at 400 bars for a super-cooling of about 35 K. The TIP4P/ICE model and a Lennard-Jones center were used for water and methane, respectively. To estimate the nucleation rate, the seeding technique was employed. Clusters of the methane hydrate of different sizes were inserted into the aqueous phase of a two-phase gas–liquid equilibrium system at 260 K and 400 bars. Using these systems, we determined the size at which the cluster of the hydrate is critical (i.e., it has 50% probability of either growing or melting). Since nucleation rates estimated from the seeding technique are sensitive to the choice of the order parameter used to determine the size of the cluster of the solid, we considered several possibilities. We performed brute force simulations of an aqueous solution of methane in water in which the concentration of methane was several times higher than the equilibrium concentration (i.e., the solution was supersaturated). From brute force runs, we infer the value of the nucleation rate for this system rigorously. Subsequently, seeding runs were carried out for this system, and it was found that only two of the considered order parameters were able to reproduce the value of the nucleation rate obtained from brute force simulations. By using these two order parameters, we estimated the nucleation rate under experimental conditions (400 bars and 260 K) to be of the order of $\log_{10} (J/(m^3 s)) = -7(5)$.

Published under an exclusive license by AIP Publishing. https://doi.org/10.1063/5.0132681

I. INTRODUCTION

Water and methane are not miscible. When the mixture is cooled at constant pressure, a solid phase (known as methane hydrate) can be formed below a certain temperature denoted as T_3.[1] At the triple point temperature T_3 (which depends on pressure), one has three phases at equilibrium, namely, a gas phase, an aqueous phase, and a solid phase of the hydrate. Below T_3, one should have again two phases, a solid hydrate and another fluid phase (water or methane gas depending on the global composition of the system). Methane hydrates present a cubic sI structure,[1,2] where molecules of methane occupy the cavities formed by a network of molecules

of water connected via hydrogen bonding. Since the formation of a solid phase is an activated process that must overcome a free energy barrier, it is possible to find the gas in contact with the fluid phase even at temperatures below T_3. In this case, the two-phase system formed by the gas and aqueous phase is metastable with respect to a system having also two phases but containing the hydrate and another phase. Often, the presence of impurities or solid surfaces induces the formation of the solid phase. This is denoted as heterogeneous nucleation. However, in the absence of impurities or surfaces, the nucleation is homogeneous.[3] In homogeneous nucleation, an embryo of the new phase (hydrate in this case) is formed

spontaneously via a fluctuation, and when it is larger than a certain critical size, it provokes the growth of the solid phase. Therefore, the formation of a solid occurs via a nucleation and growth mechanism.

A critical magnitude in nucleation studies is the nucleation rate J, which represents the number of critical clusters formed per unit of volume and per unit of time. Since the critical cluster is formed in the aqueous phase, the volume to consider for nucleation studies of hydrates is the volume of the aqueous phase. A number of experimental studies have provided nucleation rates for the formation of ice.[4–13] In addition, a number of computer simulation studies have considered this problem in detail.[14–22] Although we do not have a complete consensus about the values of nucleation rates for the formation of ice, and some problems are still not fully understood, at least we have an initial understanding of the global picture.[23] However, in the case of hydrate nucleation, our understanding of the values of homogeneous nucleation rates is still limited.[24,25]

First, experimental studies on hydrate nucleation are quite scarce and show lack of agreement.[26–33] Similarly, computational studies[34–50] are scarce and often performed under conditions that are not close to those performed in experiments. Pioneering computational studies on hydrate nucleation used an interesting strategy. They employed aqueous solutions with a concentration of methane much higher than that found in experimental studies. In experimental studies, the concentration of methane is determined by the equality of chemical potentials of methane and water in both phases (i.e., gas and aqueous phases). The interface between these two immiscible phases is planar. The value of the molar fraction of methane in the aqueous phase when in equilibrium with the gas phase via a planar interface is usually denoted as the "solubility," i.e., $x^0_{CH_4}$. However, in simulation studies, there are two common strategies to increase the concentration of methane above $x^0_{CH_4}$. In the first case, one performs simulation studies of a system having a homogeneous aqueous phase with an extremely high concentration of methane (thus, the aqueous solution is supersaturated with methane and has a methane concentration many times higher than that found at equilibrium conditions). Under these circumstances, the nucleation of the hydrate occurs in timescales of the order of hundreds of nanoseconds or less.[34,36] Note that this strategy is successful only at low temperatures where the nucleation of gas bubbles occurs in a much larger timescale, as we have shown recently.[51] The second strategy is more subtle. One has a two phase system (water and gas), but instead of having a planar interface, methane molecules form a spherical bubble, which results in an increase of the solubility of methane molecules in the aqueous phase.[37–40] Using these two strategies (which increase the concentration of methane with respect to $x^0_{CH_4}$), one can nucleate hydrates spontaneously at low temperatures by using brute force (BF) simulations.[34,36,40] Note that in brute force simulations, the nucleation rate is of the order of $10^{30-33}/(m^3 \text{ s})$ as the volume of the sample is of the order of 10–100 cubic nanometers and the observation time is of the order of a few microseconds.[15,52] However, nucleation rates found in experiments are typically in the range 10^{0-14} for observation times of minutes and sample sizes between 10^{-3} and 10^{-17} m³.[3,23] The summary is that brute force simulation studies cannot provide estimates of nucleation rates found in experiments for one reason: they require an extremely high driving force (i.e., chemical potential difference between the solid and the molecules of methane and water in the fluid phase), and this can only be achieved either by performing

studies at extremely low temperatures or with the use of extremely supersaturated solutions that cannot be achieved in experiments.

To estimate nucleation rates under conditions closer to the experiment, one should use rare event techniques.[53–58] In fact, Bolhuis and co-workers[37–39] and Barnes et al.[45] have started this route. In an attempt to obtain results closer to the experiment, Bolhuis and co-workers used transition path sampling,[53,59] and they were able to estimate nucleation rates at temperatures much closer to T_3 than any other study before. However, to keep the calculations within reasonable limits, a bubble of methane was used as a gas reservoir, and therefore, the solubility of methane in water was higher than that found for a planar interface. It should be mentioned that the role of nanobubbles in hydrate nucleation is not fully understood.[60,61] It is not clear if nanobubbles could play an important role. Further work is needed. For instance, nanobubbles could be responsible for the so-called memory effect of hydrate nucleation (i.e., the experimental evidence that the nucleation of the hydrate is much easier in a system where the hydrate was formed previously).[30,62–64] Leaving aside the role of nanobubbles, it seems of interest to estimate the nucleation rate of hydrates under usual experimental conditions (ECs). What do we mean by experimental conditions? We mean that there are no bubbles of gas in the system and the concentration of methane in water is the equilibrium one, i.e., $x^0_{CH_4}$. The equilibrium concentration is the one that would be obtained by using a planar interface so that both the methane and aqueous phases have the same pressure (when having bubbles, the pressure of methane in the bubble is higher than that of the aqueous phase).

In this work, we shall try to estimate the nucleation rate of the methane hydrate under experimental conditions. We shall use the TIP4P/ICE force field[65] for water and the single Lennard-Jones (LJ) site model[66,67] for methane, which are able to provide quite good estimates of T_3 as compared to experiments.[51] To determine J, we shall use the seeding technique.[68]

Seeding studies started with the work of Bai and Li;[69,70] it is also in the spirit of the work of Carignano and co-workers[71] and was more officially presented in the work of Knott et al.[35] and Sanz et al.[14] In the paper of Knott et al., the nucleation rate for the formation of a hydrate was considered, while in the paper of Sanz et al., the nucleation rate for the formation of ice was determined. The technique of Seeding has been applied since then to a number of different systems, starting from simple models as hard spheres (HSs),[68,72–74] Lennard-Jones (LJ),[68,75] and evolving toward much more complex systems.[14,35,76–79] The aim of this study is to provide a reasonable estimate of the value of the homogeneous nucleation rate under experimental conditions, namely, a pressure of 400 bars and a supercooling of 35 K.

II. METHODOLOGY

A. Seeding: A brief description

Classical Nucleation Theory (CNT) is a theoretical framework, aimed to obtain nucleation rates J. The work of Volmer and Weber[80] and of Becker and Döring[81] leads to the well-known expression (for the particular case of freezing),[82]

$$J = \rho_f Z f^+ e^{(-\beta \Delta G_c)} = \rho_f \sqrt{\frac{|\Delta G''_c|}{(2\pi k_B T)}} f^+ e^{(-\beta \Delta G_c)}, \quad (1)$$

where ρ_f is the number density of molecules in the fluid phase, Z is the Zeldovich factor, f^+ is the attachment rate, $\beta = 1/(k_B T)$, ΔG_c is the free energy barrier for nucleation, and $\Delta G_c''$ is the curvature (i.e., second derivative) of the free energy profile at the maximum.

This theory has undergone a second renaissance after the work of Frenkel and co-workers.[83–86] They showed that all the quantities in the previous equation can be obtained from computer simulations. The key idea is to evaluate the free energy as a function of an order parameter describing the transition (typically, the size of the largest cluster), determining its maximum (which is just ΔG_c) and the curvature at the maximum (which allows us to compute Z). The other parameters, ρ_f and f^+, are obtained from additional simulations (ρ_f from NpT runs of the fluid phase and f^+ from runs starting at the top of the free energy barrier from which the diffusion coefficient in the one-dimensional space of the order parameter can be determined). This approach is usually denoted as umbrella sampling (US)[55,56] as this technique is used to determine the free energy barrier and has led to an exceptional improvement in our understanding of freezing and in determining nucleation rates for systems such as HS,[83,87] LJ,[88] water (mW),[89] Si,[90] NaCl,[91] and many others. It is important to point out that in US, one directly obtains the free energy barrier and its value is hardly affected by the choice of the order parameter selected to describe the transition (provided that it is reasonable), as has been found for HS in the work of Filion et al.[87] and for LJ and the mW model of water[92] in the work of Prestipino.[93] Although US is certainly elegant and almost an exact technique, it is computationally quite demanding when the size of the critical cluster is large, which happens as one approaches the region where experimental values of J are reported.

Around ten years ago, a new approach for studying nucleation was presented and received the name of seeding. This technique, as US, uses Eq. (1) to estimate nucleation rates and also uses the input from computer simulations. If this is so, what is the difference between seeding and US? The main difference is that in seeding, one does not compute ΔG_c but rather the size of the critical cluster N_c using the fact that a critical cluster melts or grows with equal probability. If the size of the cluster is smaller than the critical size, in most of the runs, the solid cluster will melt, while if the cluster is larger than the critical size, growth of the solid cluster will be observed in most cases. Thus, clusters are inserted at certain T and p into the liquid phase, and one determines the size of the cluster for which the probabilities of melting and growing are equal. However, N_c does not enter in Eq. (1) so that it is not clear how this can help. The key is now to use the thermodynamic formalism for nucleation developed by Gibbs[94] (the thermodynamic ingredient) to connect ΔG_c and N_c using the following equations:

$$\Delta G_c = \frac{N_c \cdot |\Delta\mu|}{2}, \qquad (2)$$

$$\frac{|\Delta G_c''|}{2\pi \cdot k_B T} = \frac{|\Delta\mu|}{6\pi \cdot k_B T \cdot N_c}, \qquad (3)$$

where $\Delta\mu$ (for a pure component) is the difference in chemical potential between a bulk solid and a bulk fluid at the same T and p, which is easily obtained using thermodynamic integration from the coexistence point where $\Delta\mu = 0$. Seeding eliminates the need for performing free energy calculations by replacing them with a much

simpler determination of the size of the critical cluster. However, the seeding technique presents a problem. The size of the critical cluster depends on the choice of the order parameter, and therefore, although the value of ΔG_c is unique, different choices of the order parameter will lead to different estimates of its magnitude.[78] It can be shown that there is a particular choice of the order parameter that provides an exact value of ΔG_c (in particular, the one that leads to the exact determination of the radius of the cluster at the surface of tension[95–98]). Although the value of this radius is unknown, at least we know that there is a particular choice of the order parameter that provides a good estimate of ΔG_c. The summary is that seeding should be used with care. If possible, one should use an order parameter that reproduces results from more rigorous routes either for ΔG_c and/or for J, as, for instance, those obtained from umbrella sampling, Forward Flux Sampling[99] (FFS), or brute force simulations. In previous work,[14,15,77] we have shown that an empirical criterion denoted as "mislabeling" combined with the order parameter proposed by Lechner and Dellago[100] to identify molecules as fluid or solid was able to describe quite well the nucleation rates obtained for a number of pure component systems, such as HS, LJ, water, and NaCl.

In this work, we shall use seeding to describe the nucleation of the hydrate from an inhomogeneous system consisting of water and methane. Our approach will be similar to that developed by Knott et al.[35] However, we will pay special attention to the choice of the order parameter by selecting one that is able to reproduce nucleation rates obtained from brute force simulations.

The working expressions of J that we shall use in this work are

$$J = \rho_{liquid}^{\mathrm{CH_4}} \cdot Z \cdot f_{\mathrm{CH_4}}^+ \cdot \exp\left(\frac{-N_c^{\mathrm{CH_4}} \cdot |\Delta\mu_{nucleation}|}{(2 \cdot k_B T)}\right), \qquad (4)$$

$$Z = \sqrt{\frac{|\Delta\mu_{nucleation}|}{6\pi \cdot k_B T \cdot N_c^{\mathrm{CH_4}}}}, \qquad (5)$$

where the density of molecules of methane in the fluid phase is $\rho_{liquid}^{\mathrm{CH_4}}$, $N_c^{\mathrm{CH_4}}$ is the size of the critical cluster (expressed as the number of molecules of methane in the critical cluster), Z is the Zeldovich factor, $\Delta\mu_{nucleation}$ is the driving force for the formation of the hydrate (it will be described in detail in Sec. II B), and $f_{\mathrm{CH_4}}^+$ is the attachment rate that can be estimated as[101]

$$f_{\mathrm{CH_4}}^+ = \frac{\left\langle \left(N_c^{\mathrm{CH_4}}(t) - N_c^{\mathrm{CH_4}}(t_0)\right)^2 \right\rangle}{2 \cdot t}, \qquad (6)$$

where $N_c^{\mathrm{CH_4}}(t)$ is the cluster size at time t and $N_c^{\mathrm{CH_4}}(t_0)$ is the size of the cluster at $t = 0$.

B. The driving force for the nucleation $\Delta\mu_{nucleation}$

One can regard the formation of the hydrate as a chemical reaction[102] so that

$$\mathrm{CH_4}(aq, x_{\mathrm{CH_4}}) + 5.75\ \mathrm{H_2O}(aq, x_{\mathrm{CH_4}})$$
$$\rightarrow [\mathrm{CH_4}(\mathrm{H_2O})_{5.75}]_{hydrate}, \qquad (7)$$
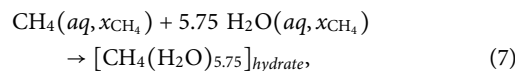
where methane in the aqueous phase reacts with 5.75 molecules of water to form the hydrate. In a unit cell of the hydrate, there are 46

molecules of water and eight molecules of methane. We shall assume the full occupancy of the cages of the hydrate, which gives the water to methane ratio equal to 5.75, hence the factor of 5.75 in Eq. (7). We shall denote as $\Delta\mu_{nucleation}$ the chemical potential change for this process,[102,103]

$$\Delta\mu_{nucleation} = \mu_{hydrate} - \mu_{CH_4}(aq, x_{CH_4}) - 5.75 \cdot \mu_{H_2O}(aq, x_{CH_4}), \quad (8)$$

where $\mu_{CH_4}(aq, x_{CH_4})$ and $\mu_{H_2O}(aq, x_{CH_4})$ are chemical potentials of methane and water in the aqueous phase, respectively. Even though the hydrate is formed out of two different molecules, since its composition is fixed (assuming the full occupancy of the cages of the hydrate), it can be treated as a single species, and hence, its chemical potential can be defined as a sum of chemical potentials of its individual components,

$$\mu_{hydrate} = \mu_{CH_4}(solid, x_{CH_4}) + 5.75 \cdot \mu_{H_2O}(solid, x_{CH_4}). \quad (9)$$

From a thermodynamic point of view, the formation of the hydrate is possible when the condition

$$\Delta\mu_{nucleation} < 0 \quad (10)$$

is satisfied. Let us discuss when this condition is satisfied. In Fig. 1, we present a sketch of the changes (at constant pressure) of the solubility of methane in water with temperature when in contact with the hydrate or when in contact with the gas (in both cases via a planar interface). In fact, we have recently computed both solubility curves at 400 bars for the force field used in this work.[51] The crossing of the two solubility curves determines the triple point temperature T_3 as has been previously shown.[51,104] Along the solubility curve of the hydrate, it holds that $\Delta\mu_{nucleation} = 0$. Thus, this line separates the region where the formation of the hydrate is possible (above this line) from the region where it is not possible (below this line) from a thermodynamic point of view.
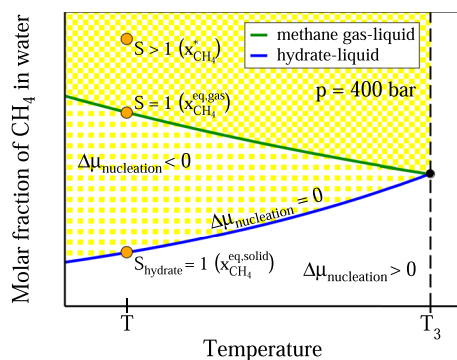

FIG. 1. Schematic depiction of the regions of temperature and molar fraction of methane in water where the nucleation of the methane hydrate is possible (entire yellow region) and not possible (non-yellow region). Solid lines represent solubility values of methane in water at different temperatures below T_3 from gas–liquid (green line) and solid–liquid (blue line) systems with planar interfaces. In the yellow region, above the solubility line from the gas phase (dark yellow), the system is in a doubly metastable state where one can have the nucleation of either gas phase or the hydrate. In the entire yellow region (light and dark), the thermodynamically stable state is the hydrate in equilibrium with a fluid phase.

It is interesting to define two types of supersaturations at certain T and p,

$$S_{hydrate} = x_{CH_4}/x_{CH_4}^{eq,hydrate} \quad (11)$$

and

$$S = x_{CH_4}/x_{CH_4}^{eq,gas} = x_{CH_4}/x_{CH_4}^0, \quad (12)$$

where x_{CH_4} is the actual concentration of methane in the aqueous phase, $x_{CH_4}^{eq,gas}$ is the solubility of methane in water when in contact with the gas via a planar interface (at T and p), and $x_{CH_4}^{eq,hydrate}$ is the solubility of methane in water when in contact with the hydrate via a planar interface (at T and p). For simplicity, we shall denote $x_{CH_4}^{eq,gas}$ as $x_{CH_4}^0$ and values of x_{CH_4} larger than $x_{CH_4}^0$ will be labeled with an asterisk ($x_{CH_4}^*$). The formation of the hydrate is possible from a thermodynamic point of view when $S_{hydrate} > 1$ and not possible when $S_{hydrate} < 1$. Sometimes, in the literature, $S_{hydrate}$ is denoted as S, and for this reason, it is necessary to read carefully the definition of S in each individual paper.

Let us focus on the particular case of the nucleation of the hydrate at 260 K and 400 bars. How to perform experiments on the nucleation under these conditions? The simplest approach is to have a container where both water and methane are in contact via a planar interface and to cool the system to the temperature of 260 K while keeping the pressure at 400 bars. We shall denote this approach as "experimental conditions" (ECs), and it has been the way experiments have been performed in several studies.[24,105,106] In this work, we would like to mimic this way of doing experiments. However, we will only consider the possibility of the nucleation in the bulk of the aqueous phase (i.e., homogeneous nucleation) and we shall not consider the possibility of the hydrate formation at the interface (heterogeneous nucleation). The possibility of using seeding to investigate heterogeneous nucleation is interesting and deserves to be explored in more detail in the future. However, there are other possible ways of doing experiments. In fact, one could have a sample of water into which a certain amount of methane is introduced so that $S < 1$ while $S_{hydrate} > 1$. Under these circumstances, the formation of the hydrate is still possible from a thermodynamic point of view, but one does not have enough methane to generate the gas phase so that there will be no interface. In this case, the only mechanism for hydrate formation will be homogeneous nucleation (which could be relevant to the hydrate formation in the sea[107]).

The summary is that although usually experiments are performed at $S = 1$ while having two phases in contact via a planar interface, it would be possible to perform experiments with $S < 1$ when having only one phase (the hydrate would still be the stable phase, provided that $S_{hydrate} > 1$). It should be mentioned that it is also possible to have only one phase even when $S > 1$. In this case, the system is in a doubly metastable state (with respect to the formation of the hydrate and with respect to the formation of the gas phase). The transition with the fastest kinetics will occur first (see our previous work[51] for a more detailed discussion of this). In fact, as will be shown in this work, for systems with values of S as large as 4.72 and 5.62, the formation of the hydrate occurs first and we do not observe the formation of the gas phase.

The particular values of $x_{CH_4}^{eq,gas}$ and $x_{CH_4}^{eq,hydrate}$ at 260 K and 400 bars found in our previous work[51] for the force field of this work are

0.0089 and 0.0009, respectively. Values of $\Delta\mu_{nucleation}$ at 400 bars for the model of this work have also been reported by us[51] recently using several thermodynamic routes. A particularly simple but approximate route to determine $\Delta\mu_{nucleation}$ of the hydrate (denoted as route 2 in our previous work) is to use

$$\frac{\Delta\mu_{nucleation}}{k_B T} \simeq \ln\left(\frac{x_{CH_4}}{x_{CH_4}^{eq,hydrate}}\right) = \ln(S_{hydrate}) \qquad (13)$$

although due to the extremely low value of $x_{CH_4}^{eq,hydrate}$ this route has larger uncertainties than other possible routes, as was discussed in our previous work.[51] We have also shown[51] that values of $\Delta\mu_{nucleation}$ around 4 (in $k_B T$ units) are sufficient to induce nucleation in brute force (BF) runs. Note that Eq. (13) can also be used to determine the value of $\Delta\mu_{nucleation}$ of a gas phase if the value of $x_{CH_4}^{eq,gas}$ is used instead of $x_{CH_4}^{eq,hydrate}$ in the denominator of Eq. (13).

Another route to estimate the value of $\Delta\mu_{nucleation}$ can be obtained by assuming that the enthalpy of dissociation of the hydrate does not change with temperature and can be taken as the value at T_3. By neglecting the change of the composition of the solution with temperature, one can obtain a simple expression,

$$\Delta\mu_{nucleation} \simeq \frac{h_{diss}^{T_3}}{T_3}(T - T_3) = s_{diss}^{T_3}(T - T_3), \qquad (14)$$

where $h_{diss}^{T_3}$ is the enthalpy of dissociation at T_3 and $s_{diss}^{T_3}$ is the entropy of dissociation at T_3. Using the values of $h_{diss}^{T_3}$ = 48.12 kJ/mol and T_3 = 295 K that we have obtained previously,[51] we obtain $s_{diss}^{T_3}$ = 163 J/(mol K). We have also included a figure in the supplementary material with the values of $\Delta\mu_{nucleation}$ from Eq. (14) [note that we found an error in Fig. 10 of our previous work[51] when implementing Eq. (14)]. In any case, both Eqs. (13) and (14) are approximate, and there are other ways of estimating $\Delta\mu_{nucleation}$ with higher accuracy as discussed in our previous work.[51] In Sec. II C, we shall provide the details of simulation runs.

C. Simulation details

All the calculations presented in this paper were obtained with the use of classical molecular dynamics (MD). Simulations were carried out using the GROMACS[108,109] package. The NpT ensemble was used in all cases. Depending on the system characteristics, either isotropic NpT (all sides of the simulation box change proportionally) or $Np_z T$ (only one side of the simulation box changes) ensemble was used. The pressure was kept constant with the use of the Parrinello–Rahman barostat,[110] while the temperature was kept constant with the use of the Nosé–Hoover thermostat.[111,112] In both cases, the relaxation time of the barostat and thermostat constants used was equal to 2 ps. A time step of 2 fs was used for all simulations. A cutoff of 9 Å was used for both electrostatic and van der Waals interactions. For Coulombic interactions, the Particle Mesh Ewald (PME) method was employed. Long range energy corrections to energy and pressure were applied to the Lennard-Jones part of the potential. The TIP4P/ICE[65] model was used for water, while parameters of Refs. 66 and 67 were used for methane. Lorentz–Berthelot combination rules were applied for cross-interactions between TIP4P/ICE and methane models. The LINCS[113,114] algorithm was used to maintain the geometry of water molecules in the systems.

Two types of simulations were carried out. First, brute force simulations of supersaturated solutions of methane in water were conducted at 260 K and 400 bars in an isotropic NpT ensemble [see Fig. 2(a)]. Second, seeding was used in order to obtain systems in which a spherical cluster of methane hydrate was immersed in a liquid solution of methane in water. Spherical clusters of the solid were inserted into either a one-phase liquid system [Fig. 2(b)] or a two phase gas–liquid system [Fig. 2(c)]. Both systems were equilibrated before the seeding procedure was used to introduce a cluster of the solid into the liquid phase. The equilibration was carried out at 260 K and 400 bars for about 100 ns, in either the isotropic NpT or $Np_z T$ ensemble, depending on the system.

In order to obtain a spherical cluster of a methane hydrate, a simulation of a bulk hydrate under the considered temperature and pressure conditions (400 bars and 260 K, 1242 molecules of water and 216 molecules of methane) was carried out. The structure of a methane hydrate was sI structure ($Pm\bar{3}n$),[1,2] with a lattice constant equal to about 12 Å. Oxygen atoms of water molecules occupy crystallographic positions c (6 molecules), k (24 molecules), and i (16 molecules), while methane molecules occupy d (6 molecules) and a (2 molecules) positions.[2] In our simulations, we assumed a full occupancy of the cages, meaning that methane molecules were present
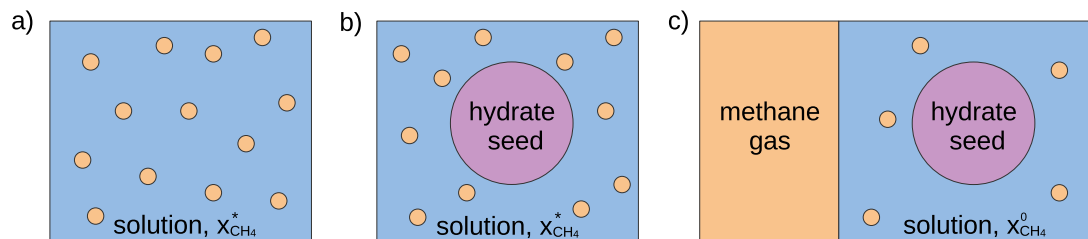
FIG. 2. Schematic depiction of simulation systems used in this study. Isotropic NpT simulations were used in cases (a) and (b), whereas anisotropic $Np_z T$ was used in case (c) where the z axis is perpendicular to the interface. (a) A homogeneous supersaturated solution of methane in water ($x_{CH_4}^*$). (b) A homogeneous supersaturated solution of methane in water ($x_{CH_4}^*$) into which a spherical cluster of the methane hydrate was introduced. (c) Two-phase gas–liquid system, where the methane gas is in contact with the solution of methane in water via a planar interface, into which a spherical cluster of a methane hydrate was inserted. The concentration of methane in the liquid phase is equal to the equilibrium solubility under the studied conditions (260 K and 400 bars), $x_{CH_4}^0$.

in all cages formed by water molecules. In experiments, occupancies around 95% are often found.[1,115] Proton disorder satisfying the Bernal–Fowler rules[116] was introduced to the system, with the use of the algorithm of Buch *et al.*[117]

After the equilibration of the bulk solid, a spherical cluster of a certain radius was cut out from the system. The cluster was then inserted into the liquid phase of either the one-phase liquid system or the two-phase gas–liquid system. The molecules of the liquid phase that were overlapping with the molecules of the inserted cluster (i.e., were closer than 0.5 nm away from any molecule of the cluster) were removed from the system. As a result of this procedure, an empty space around the cluster was created. In order to fill this space with molecules of liquid, short equilibration runs were performed. In the case of seeding into a one-phase liquid system, a 1 ns run in the NVT ensemble was carried out. After that, a short equilibration run (1 ns) in the NpT ensemble was also carried out in order to restore a correct pressure in the system. For the seeding into a two-phase gas–liquid system, the solid cluster was inserted in the middle of the liquid phase and the equilibration was performed in the Np_zT ensemble (with z being the direction perpendicular to the planar gas–liquid interface) for 1.5 ns. In both cases, the equilibration time was kept short enough so that no significant changes of the size of the cluster inserted into the liquid could occur. At the same time, it was long enough to equilibrate the solid–liquid interface (as we already mentioned, bulk phases were equilibrated separately before the insertion of the seed the into liquid). A similar approach was successfully used before in the case of ice Ih using the seeding technique.[14,15] The production runs of the systems were carried out at 400 bars and 260 K in either the isotropic NpT (seeding into supersaturated solutions of methane in water) or Np_zT (seeding into a two phase gas–liquid system) ensemble.

III. RESULTS

A. The choice of the order parameter

For seeding, we shall use as the order parameter the size of the largest solid cluster. Since the methane hydrate is a two component system, when determining the size of the solid cluster, one could use either methane or water molecules. In general, in this work, we shall use the molecules of water for that purpose. Molecules of water will be identified as liquid or solid according to a certain order parameter. We will assume that two molecules of water labeled as solid are connected (so that they belong to the same solid cluster) if their distance (between the oxygen atoms) is smaller than 3.5 Å. The number of molecules of methane in the solid cluster will be obtained by simply dividing by 5.75 the number of solid molecules of water. We have used in the past the order parameters developed by Lechner and Dellago[100] when considering the nucleation of ice so that it seems a natural choice. In our recent work,[51] we have shown that the $\overline{q_3}$ order parameter is able to distinguish reasonably well between the molecules of water in the fluid and in the solid hydrate. When determining the values of $\overline{q_3}$, we considered all molecules of water within 5.5 Å from the molecule of interest (being 5.5 Å the distance between their oxygen atoms). The threshold value for $\overline{q_3}$ will be obtained using the mislabeling criterion as described in our recent paper.[51] Note that only oxygen atoms are considered when evaluating the order parameter for water. To test the impact of the choice of the order parameter on the size of the solid cluster of the

methane hydrate, we chose four other additional order parameters. Instead of using simply $\overline{q_3}$, we computed simultaneously two order parameters for each molecule of water, namely, $\overline{q_3}$ and $\overline{q_5}$. We again implemented the mislabeling criterion, but now using a linear combination of $\overline{q_3}$ and $\overline{q_5}$. In addition to that, we shall also introduce a modified version of $\overline{q_3}$ order parameter (which we will refer to as $\overline{q_{3\,scaled}}$). The last parameter that we implement is the $\overline{q_{12}}$ order parameter. All these parameters label water molecules as either solid or liquid. Finally, we shall use the popular Mutually Coordinated Guest (MCG) order parameter,[118] which analyzes the ordering of the molecules of methane rather than that of water.

First, let us discuss the differences between $\overline{q_3}$, the linear combination of $\overline{q_3}$ and $\overline{q_5}$, and $\overline{q_{3\,scaled}}$ order parameters. In Fig. 3, values of $\overline{q_3}$ and $\overline{q_5}$ order parameters are plotted for water molecules in a bulk solid (methane hydrate simulated at 260 K and 400 bars, blue points) and a bulk liquid (solution of methane in water, 260 K, 400 bars, green points). It can be clearly seen that the points corresponding to different phases create separate clouds. Using suitable cut-off values, water molecules can be assigned to solid or liquid phases. In the case of $\overline{q_3}$ order parameter, water molecules are assigned as solid if the
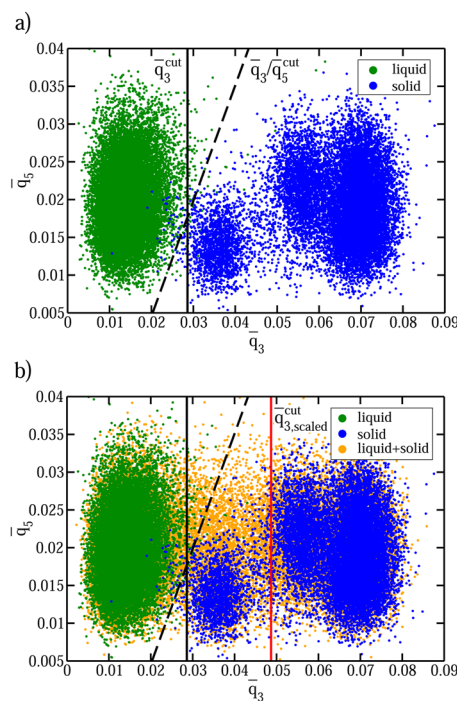
FIG. 3. Values of $\overline{q_3}$ and $\overline{q_5}$ order parameters of individual water molecules (their oxygen atoms) in systems simulated at 260 K and 400 bars. (a) Results obtained with the use of $\overline{q_3}$ and $\overline{q_5}$ for purely liquid (solution of methane in water at $x^0_{CH_4}$, green points) and purely solid (methane hydrate, blue points) systems. Here, cut-off values for the $\overline{q_3}$ (black solid line) and linear combination of $\overline{q_3}$ and $\overline{q_5}$ (black dashed line) order parameters, determined with the use of the mislabeling criterion, are also presented. (b) The comparison of results obtained with the use of $\overline{q_3}$ and $\overline{q_5}$ for one-phase solid and liquid systems with results obtained for a two-phase solid–liquid system (orange points). Here, an interfacial region in between water molecules that belong to the solid and liquid phases can be clearly seen. In addition to the cutoffs represented in (a), the cutoff for the $\overline{q_{3\,scaled}}$ order parameter (red solid line) is also included.

TABLE I. Cut-off values of $\overline{q_3}$, the linear combination of $\overline{q_3}$ and $\overline{q_5}$, $\overline{q_{3\,scaled}}$, and $\overline{q_{12}}$ order parameters for 260 K and 400 bars, as determined with the use of the mislabeling criterion. The percentages of mislabeled molecules in either purely solid (methane hydrate) or purely liquid (solution of methane in water) systems obtained with the use of the considered parameters with these cut-off values are also presented.

Parameter	Cut-off value	% mislabeled
$\overline{q_3}$	0.0286	0.45
$\overline{q_3}/\overline{q_5}$	$1.528 \cdot \overline{q_3} - 0.026$	0.27
$\overline{q_{3\,scaled}}$	0.0487	<0.01
$\overline{q_{12}}$	0.121	<0.01

FIG. 4. $\overline{q_3}$ and $\overline{q_{12}}$ values for water molecules in one-phase solid (blue) and liquid (green) systems compared with results for a two-phase 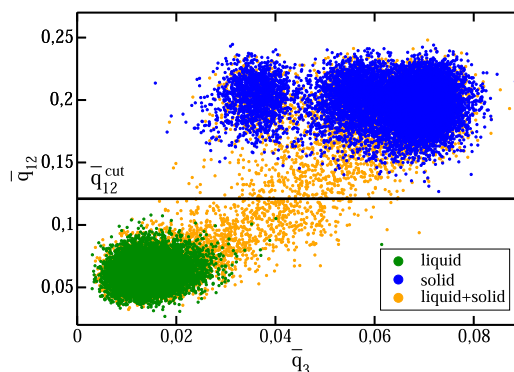solid–liquid system (orange). Here, the cut-off value for the $\overline{q_{12}}$ (black solid line), determined with the use of the mislabeling criterion, is presented.

value of $\overline{q_3}$ is higher than a certain cut-off value $\overline{q_3}^{\,cut}$, black solid line in Fig. 3(a). The accuracy of the assignment can be improved even more by using a linear combination of the values of $\overline{q_3}$ and $\overline{q_5}$ order parameters and $\overline{q_3}/\overline{q_5}^{\,cut}$ [black dashed line in Fig. 3(a)].

To evaluate the accuracy of these order parameters, we used the mislabeling criterion,[14,15] which allows us to determine the cut-off values that give the lowest percentage of molecules of water that are labeled incorrectly. The mislabeling criterion requires the same percentages of wrong labeling in both phases. For the systems considered in this work, cut-off values obtained for 260 K and 400 bars, along with the percent of mislabeled molecules of water, are presented in Table I.

As can be seen, both $\overline{q_3}$ and the linear combination of $\overline{q_3}$ and $\overline{q_5}$ parameters work well for distinguishing water molecules in solid and liquid phases, when one-phase systems are considered. However, as shown in Fig. 3(b), in a two-phase solid–liquid system (orange points), there is no clear border between water molecules that belong to solid and liquid phases. An interfacial region can be clearly observed, in which water molecules cannot be unambiguously assigned as solid or liquid using $\overline{q_3}$ and the linear combination of $\overline{q_3}$ and $\overline{q_5}$ order parameters. It is also clear from Fig. 3 that the size of a solid cluster immersed in a liquid solution can be significantly different depending on which of the two parameters is used.

In order to limit the impact of the choice of the way in which water molecules belonging to the interfacial region are assigned as solid or liquid, we propose a modification of the $\overline{q_3}$ order parameter—the $\overline{q_{3\,scaled}}$ order parameter. As can be seen in Fig. 3, water molecules that belong to the solid phase (in the case of a purely solid system, blue points) are arranged in three clouds. These clouds represent the oxygen atoms that occupy three different crystallographic positions in the sI ($Pm\bar{3}n$) hydrate structure. The cloud that is the closest to the liquid water region is representing oxygen atoms that occupy the crystallographic positions of type c in the solid, and the other two clouds represent the k and i crystallographic positions. Knowing that there are 46 water molecules in a unit cell of the sI hydrate and there are six molecules of water that occupy type c crystallographic positions, we can find the size of the cluster of a hydrate in the liquid by assigning water molecules for which the values of $\overline{q_3}$ are higher than certain $\overline{q_{3\,scaled}}^{\,cut}$ [red solid line in Fig. 3(b)] and multiplying the obtained number by the factor of 46/40. In Table I, we presented the results of the mislabeling for the $\overline{q_{3\,scaled}}$ order parameter. As can be seen, for the one-phase systems, the accuracy of the parameter is even higher than for $\overline{q_3}$ and the linear combination of $\overline{q_3}$ and $\overline{q_5}$ order parameters.

Apart from the parameters described above, we also implemented the $\overline{q_{12}}$ order parameter. The reason for this choice is that we analyzed the performance of the order parameters of Lechner and Dellago from $\overline{q_3}$ to $\overline{q_{20}}$ (considering as neighbors molecules at less than 5.5 Å) and concluded that $\overline{q_{12}}$ provided the smallest value of the mislabeling (i.e., percentage of molecules in the fluid phase labeled as hydrate and of molecules in the hydrate labeled as fluid). Further work is needed to understand the reasons (geometrical) that make $\overline{q_{12}}$ so efficient in identifying the water molecules of the hydrate. As can be seen in Table I and Fig. 4 (blue and green points), the $\overline{q_{12}}$ order parameter separates molecules of water in the hydrate from molecules of water in the liquid quite well. The mislabeling is reduced significantly with respect to the $\overline{q_3}$ and the linear combination of $\overline{q_3}$ and $\overline{q_5}$ order parameters. Again, when there is an interface (orange points), interfacial molecules of water adopt values of the order parameter intermediate between those of the hydrate and liquid water.

In contrast to parameters described above, the MCG[118] order parameter uses methane molecules in order to estimate the content of the solid phase in a system. A set of geometrical criteria is used to determine whether a certain molecule of methane belongs to the solid or liquid phase. In order for a molecule of methane to be considered solid, it has to have a minimum number of neighboring methane molecules in a distance shorter or equal to 0.9 nm. Additionally, between the considered methane molecule and the neighboring methane molecules, at least five molecules of water have to be present (for each pair of methane molecules). The minimum number of the neighboring molecules of methane that satisfy the above-mentioned criteria can be equal to 1 (MCG-1 order parameter) or 3 (MCG-3 order parameter). The use of a more strict criterion in the case of the MCG-3 order parameter allows us to determine the size of a well-defined solid structure, in contrast to the MCG-1 order parameter, which takes into account also less ordered, interfacial molecules of methane. For that reason, we shall use MCG-3 in this work.

In order to compare the five order parameters described above, we determined the size of a spherical cluster of the methane hydrate

TABLE II. The average size of the largest cluster in a system containing a stable cluster of a methane hydrate immersed in a liquid solution of methane in water (see Fig. 7 of our previous work[51]) obtained with the use of five different order parameters: $\overline{q_3}$, linear combination of $\overline{q_3}$ and $\overline{q_5}$, $\overline{q_{3\,scaled}}$, $\overline{q_{12}}$, and MCG-3. The size of the cluster is presented as a number of molecules of water in the cluster N^{H_2O} and as a number of molecules of methane in the cluster N^{CH_4}. In order to convert the size of the cluster between N^{H_2O} and N^{CH_4}, we used the expression $N^{H_2O} = 5.75 \cdot N^{CH_4}$.

Parameter	N^{H_2O}	N^{CH_4}
$\overline{q_3}$	955	166
$\overline{q_3}/\overline{q_5}$	867	151
MCG-3	800	139
$\overline{q_{12}}$	679	118
$\overline{q_{3\,scaled}}$	573	100

immersed in water solution of methane, which was found to be stable in the NpT run in our previous work[51] (250 K, 400 bars)—the results are presented in Table II. It can be clearly seen that the size of the cluster of the solid detected by these order parameters differs significantly. As mentioned before, the use of the $\overline{q_3}$ order parameter gives a higher value than the linear combination of $\overline{q_3}$ and $\overline{q_5}$. The result obtained with the use of the MCG-3 order parameter is similar to the value determined by the linear combination of $\overline{q_3}$ and $\overline{q_5}$. Significantly lower values compared to the other three results were obtained using the $\overline{q_{3\,scaled}}$ order parameter. This is due to the fact that this parameter does not assign water molecules from the interfacial region as a solid phase [see Fig. 3(b)]. In comparison, the $\overline{q_{12}}$ order parameter gives values similar to those of the $\overline{q_{3\,scaled}}$, although somewhat larger.

The results presented in Table II clearly demonstrate that the choice of the order parameter largely affects the size of the cluster of the hydrate in a liquid phase. Note that in all cases, we are examining the same cluster, so differences are due to the way different order parameters see the same cluster. Based on only these results, it is not possible to predict which one of the parameters allows us to determine the size of the solid cluster that best fits CNT (i.e., provides a more accurate description of the radius of the cluster at the surface of tension). As mentioned before, the size of the critical nucleus has a huge impact on the value of the nucleation rate calculated according to Eq. (4). Therefore, the following question arises: Which order parameter should be used in order to obtain reliable values of the nucleation rate? The obvious answer for that would be the choice of such an order parameter that is able to reproduce the exact results for the considered model. Unfortunately, there is no previous rigorous results of nucleation rates of the methane hydrate that could be used as reference points. Another possibility is to conduct a molecular dynamics study of brute force nucleation from the liquid solution of methane in water. From that, the nucleation rate can be estimated using a method that is practically independent of the choice of the order parameter—this value could be then used to evaluate the suitability of different order parameters for estimating the critical nucleus size and, therefore, the nucleation rate of the hydrate, with the use of seeding.

B. Estimation of the nucleation rate from the brute force simulations

In order to estimate the rate of homogeneous nucleation of the methane hydrate, we carried out simulations of supersaturated solutions of methane in water at 260 K and 400 bars. A supersaturation of the solution of methane was required in order to increase the driving force for the nucleation so that it was possible to observe nucleation events in brute force simulations. We used systems of about $5.5 \times 5.5 \times 5.5$ nm^3 size, which contained 4942 water molecules. Two different concentrations of methane in water were considered: molar fractions of 0.042 (218 molecules of methane) and 0.05 (262 molecules of methane), which accounts for supersaturations $S = 4.72$ and $S = 5.62$, respectively [see Eq. (12)].

Even though the difference of the concentration of methane in both systems was relatively small, the time required to observe nucleation events was very different for these systems. In Fig. 5, we present changes in time of the size of the largest cluster of the methane hydrate for systems in which supersaturation was equal to 4.72 [ten independent runs, Fig. 5(a)] and 5.62 [30 independent runs, Fig. 5(b)]. The size of the largest cluster was detected with the use of the $\overline{q_{3\,scaled}}$ order parameter. As can be seen, in the case of the lower supersaturation, the time required for the system to nucleate ranges from a few hundreds of nanoseconds to a few microseconds—in some cases, we did not observe the nucleation event even after
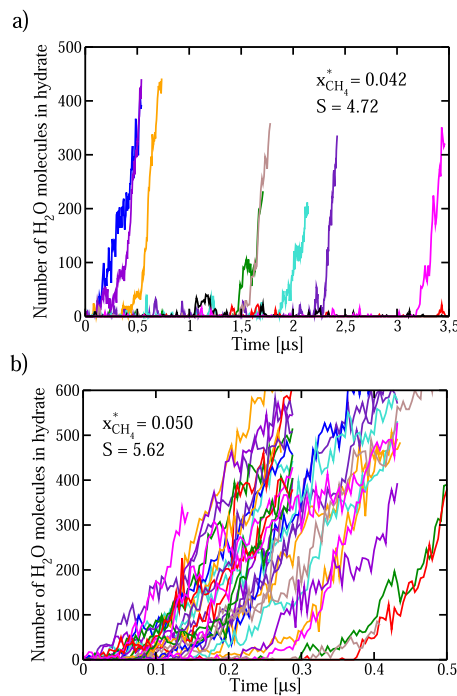
FIG. 5. Changes in time of the size of the largest cluster of a methane hydrate (as a number of water molecules in the cluster detected with the $\overline{q_{3\,scaled}}$ order parameter) in brute force NpT simulations (260 K, 400 bars) of homogeneous supersaturated solution of methane in water (a) for a supersaturation of 4.72 and (b) for a supersaturation of 5.62. The cluster size was obtained with the use of the $\overline{q_{3\,scaled}}$ order parameter. Here, the concentration of methane ($x_{CH_4}^*$) is also indicated.

3.5 μs. In order to estimate the value of the nucleation rate, we used the following equation:

$$J_{bf} = \frac{1}{\tau \cdot V} = \frac{\ln 2}{\tau_{1/2} \cdot V}, \qquad (15)$$

where τ is the average time required for the system to nucleate and V is the volume of the system equal to 159 nm^3. Out of 10 runs that we carried out for the systems at $S = 4.72$, we observed the nucleation only in 8 after 3.5 μs. For that reason, we could not determine the value of τ required for the estimation of the nucleation rate. Instead, we used the value of $\tau_{1/2}$, which is the half-time of the nucleation (time after which the nucleation was observed in a half of the considered systems). According to the first order kinetic equation, the relation between τ and $\tau_{1/2}$ is

$$\tau = \frac{\tau_{1/2}}{\ln 2}, \qquad (16)$$

which leads to the expression on the right-hand side of Eq. (15).

Using the data obtained with the $\overline{q_{3\,scaled}}$ order parameter, we estimated $\tau_{1/2}$, assuming that the nucleation occurred in a particular system if the size of the cluster of the solid was larger than 75 molecules of water (a post-critical cluster was present in the system). Note that the choice of the order parameter used to analyze the changes of the size of the solid cluster in time has little effect on the value of the nucleation time because the process of the hydrate growth is much faster than the time required for the nucleation to occur.

For the system with $S = 4.72$, we obtained the value of $\tau_{1/2}$ = 1.607 μs. Using this value, we estimated the nucleation rate using Eq. (15) obtaining $J_{bf} = 3 \cdot 10^{30}/(\text{m}^3 \text{ s})$. In the supplementary material, we have shown that the nucleation rate estimated with the use of $\tau_{1/2}$ obtained based on the $\overline{q_3}$ order parameter is consistent with this value, which confirms that the choice of the order parameter does not affect the nucleation rate obtained from brute force simulations. In order to estimate the error of the value of the nucleation rate, we repeated the calculation using $\tau_{7/10}$ instead of $\tau_{1/2}$ and implementing the method of calculating the nucleation time τ following the formula from Ref. 46. We obtained the values of J_{bf} equal to $1 \cdot 10^{30}/(\text{m}^3 \text{ s})$ and $2 \cdot 10^{30}/(\text{m}^3 \text{ s})$, respectively.

Another method for estimating the nucleation rate from brute force runs is the mean first passage time[119,120] (MFPT) method. In this method, the average time $[\tau(N)]$ in which a cluster of the solid of size N is formed for the first time in the system is estimated by averaging over all brute force trajectories. The function $\tau(N)$ can be then fitted to the following equation:[119]

$$\tau(N) = \frac{\tau_J}{2}\left[1 + erf(Z\sqrt{\pi}(N - N_c))\right], \qquad (17)$$

where τ_J is the nucleation time, Z is the Zeldovich factor, N is the size of the cluster of the solid, and N_c is the size of a critical nucleus. The results and the fit to Eq. (17) are represented in Fig. 6.

Using the value of τ_J obtained from the fitting, which is equal to 1684 ns, the nucleation rate can be obtained using the following equation (where V is the volume of the system):

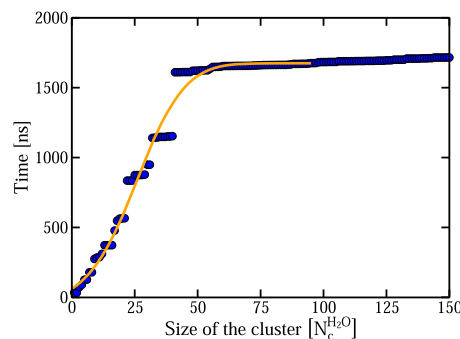$$J_{MFPT} = \frac{1}{V \cdot \tau_J}. \qquad (18)$$

FIG. 6. The results of the mean first passage time method obtained for a supersaturated solution of methane in water ($S = 4.72$) simulated at 260 K and 400 bars. For each size of the cluster $N_c^{\text{H}_2\text{O}}$ in a range of 0–150, the average time at which the cluster of that size was formed in the solution for the first time (using ten independent simulation runs) was determined. Since the nucleation occurred in only 8 out of 10 runs, we used the approach of Ref. 46 to calculate $\tau(N)$. The results were then fitted using Eq. (17) (orange solid line). From the fit, the estimated nucleation time, size of the critical cluster, and nucleation rate are $\tau_J = 1684$ ns, $N_c^{\text{H}_2\text{O}} = 26$, and $J = 4 \cdot 10^{30}/(\text{m}^3 \text{ s})$. Results were obtained using the $\overline{q_{3\,scaled}}$ order parameter.

The nucleation rate we obtain for the system with $S = 4.72$ using the MFPT method is equal to $4 \cdot 10^{30}/(\text{m}^3 \text{ s})$, which is consistent with the result obtained using the first order kinetic equation. Taking into account the four values of the nucleation rate estimated with brute force runs, the final result is $J_{bf} = 2.5(8) \cdot 10^{30}/(\text{m}^3 \text{ s})$. The MFPT method, apart from the nucleation time, provides the estimation of the size of the critical nucleus. In the case of our runs, $N_c^{\text{H}_2\text{O}} = 26$. As we will show later, this value can be used to estimate the nucleation rate using Eq. (4).

In the case of the system with a higher supersaturation, $S = 5.62$, the induction times of the formation of the hydrate were relatively short, making it difficult to distinguish between the nucleation and growth phases of the hydrate formation. For that reason, the method based on the first order kinetic equation that we used for estimating the nucleation rate in the systems with $S = 4.72$ was not applicable in this case. Therefore, in order to estimate the nucleation rate for the systems at $S = 5.62$, we employed only the MFPT method, using 30 trajectories (all of them nucleated hydrate successfully). In this case, we decided to use additionally a modified version of Eq. (17) to obtain a better fit to the data

$$\tau(N) = \frac{\tau_J}{2}\left[1 + erf(Z\sqrt{\pi}(N - N_c))\right]$$
$$+ \frac{1}{2G}(N - N_c)\left[1 + erf(C(N - N_c))\right], \qquad (19)$$

where G is the growth rate and C is a constant, which is required to be a positive number. The results and the fits using both equations are represented in Fig. 7 and Table III. Using the value of τ_J obtained from the fitting, we estimated the nucleation rate using Eq. (18)—these results are also included in Table III. As can be seen, both fits give similar values of J, which are around an order of magnitude larger than for the system with lower supersaturation ($S = 4.72$).

We have not analyzed in detail the mechanism of nucleation found in brute force simulations of this work since we are rather
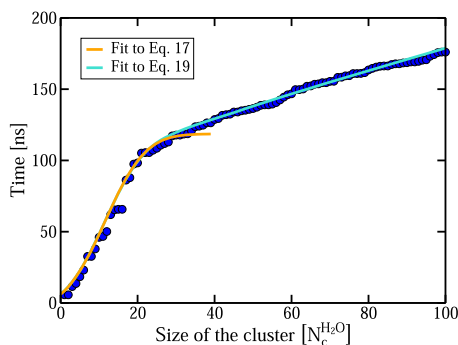
26 February 2024 09:34:05

FIG. 7. The results of the mean first passage time method obtained for a super-saturated solution of methane in water ($S = 5.62$) simulated at 260 K and 400 bars. For each size of the cluster $N_c^{H_2O}$ in a range of 0–100, the average time at which the cluster of that size was formed in the solution for the first time (using 30 independent simulation runs) was determined. The results were then fitted using Eq. (17) (orange solid line) and Eq. (19) (blue solid line). From the fits, the estimated nucleation times, sizes of the critical cluster, and nucleation rates are $\tau_J = 122.7$ ns, $N_c^{H_2O} = 11.5$, and $J = 5 \cdot 10^{31}/(m^3\ s)$ in the case of Eq. (17) and $\tau_J = 108.8$ ns, $N_c^{H_2O} = 11.0$, and $J = 6 \cdot 10^{31}/(m^3\ s)$ for Eq. (19), respectively. Results were obtained using the $\overline{q_{3\,scaled}}$ order parameter.

TABLE III. Nucleation rates in seeding runs in a supersaturated solution of methane in water ($S = 5.62$, 260 K, 400 bars) determined with the use of the MFPT method. The parameters for the fits of the data according to Eqs. (17) and (19) are also provided.

	Equation (17)	Equation (19)
τ_J (ns)	122.7	108.8
Z	0.048	0.050
$N_c^{H_2O}$	11.5	11.0
G (1/ns)	$\cdots$	1.27
C	$\cdots$	0.03
J [1/(m^3 s)]	$5 \cdot 10^{31}$	$6 \cdot 10^{31}$

interested in the nucleation rate. In a recent study,[121] the mechanism has been discussed in detail. It has also been postulated in previous work that the nucleation of the hydrate can occur via a two-step mechanism.[122,123] It is interesting to mention that for NaCl precipitation, there is a shift in the mechanism from the one step at moderate and high supersaturation to two step nucleation[124] at concentrations of NaCl above the spinodal. Further work is needed to clarify if the same could occur in the case of hydrate nucleation.

Let us finish this section by discussing a subtle issue. We are performing runs in the NpT ensemble where the number of molecules of methane and water is fixed. Since the hydrate has a relatively large molar fraction of methane (around 0.15) and the concentration of methane in the supersaturated solution is around 0.05, when the hydrate is formed and growing, the concentration of methane in the solution decreases.

However, for the initial steps of the nucleation, this is not a big problem as the critical cluster contains only around 5–10 molecules of methane and the entire system has more than 200 molecules of methane. Therefore, provided that the critical cluster is small, one should not expect big variations in the concentration of methane in

the solution in the initial stages of nucleation (of course, things are different once one is in the growth regime).

C. Estimation of the nucleation rate with the use of seeding

Seeding allows us to estimate a nucleation rate by inserting spherical clusters of solids of different sizes into a liquid and observing the change in time of the size of these clusters. As mentioned before, the size of the critical nucleus is the size of the cluster of the solid for which the probabilities of growing and melting are equal. We conducted a number of simulations of the liquid we used previously for brute force simulations ($S = 4.72$), into which we inserted spherical clusters of methane hydrates of radii in the range of 0.9–1.1 nm. The spherical clusters of solids were cut out from the system containing the methane hydrate (sI structure), which was equilibrated beforehand at 260 K and 400 bars in an anisotropic NpT ensemble. Molecules of water and methane from the original brute force system that were overlapping with the inserted seed of the hydrate were removed from the simulation box. Finally, we obtained systems consisting of around 4700–4800 molecules of water and around 200 molecules of methane and a size of $5.3 \times 5.3 \times 5.3$ nm^3. The systems were simulated at 260 K and 400 bars in the isotropic NpT ensemble for about 150 ns.

In order to follow the changes of the size of the cluster of the solid in time, we used the same order parameters that were characterized before: $\overline{q_3}$, linear combination of $\overline{q_3}$ and $\overline{q_5}$, and $\overline{q_{3\,scaled}}$, $\overline{q_{12}}$, and MCG-3. Let us present in Fig. 8 the results for only two parameters, namely, $\overline{q_{3\,scaled}}$ and MCG-3, obtained for the system in which the number of runs for which the spherical cluster inserted into the liquid solution was melting and growing was the same (r = 0.95 nm). Additionally, the results obtained for other sizes of the cluster inserted into the liquid and other order parameters are presented in the supplementary material. Results for the attachment rate using $\overline{q_{3\,scaled}}$ are represented in Fig. 9.

The sizes of the critical clusters were estimated as the average values of the sizes of clusters during the equilibration period (after the vacuum around the inserted seed was filled with liquid) in all the runs. As can be seen in Fig. 8 and Table IV, the size of the critical nucleus obtained with the use of the five order parameters differs significantly. We used these values (along with the data also presented in Table IV and in Fig. 9) to calculate the nucleation rate following the formula presented in Eq. (4)—the results are shown in Table IV.

By knowing the value of the nucleation rate obtained from brute force simulations, it is now possible to compare the results obtained by means of seeding when different order parameters are used. Recall that the brute force, unlike seeding, is not affected by the choice of a particular order parameter. The results presented in Table IV clearly show that only two of the order parameters were able to give results comparable to the one obtained by brute force simulations, namely, the $\overline{q_{3\,scaled}}$ and $\overline{q_{12}}$ order parameters. For all the other parameters, the values obtained are several orders of magnitude lower, which is a result of a significantly larger size of the critical nucleus detected with their use and thus a much higher nucleation free energy barrier. Interestingly, the free energy barrier found here using $\overline{q_{3\,scaled}}$ and $\overline{q_{12}}$ order parameters is of about 10–11 k_BT, which is similar to the one found using transition path sampling in the
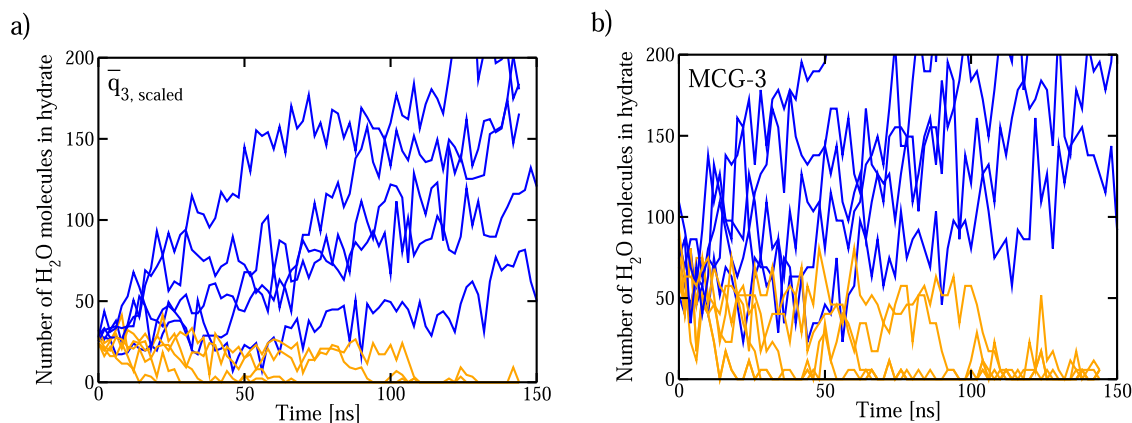
FIG. 8. Changes in time of the size of the largest cluster of a methane hydrate (as a number of water molecules in the cluster) obtained for seeding runs (260 K, 400 bars) in a supersaturated solution of methane in water ($S = 4.72$) for a seed size, which is critical under the studied conditions. The number of systems in which the cluster of the solid was growing (blue lines) or melting (orange lines) is equal to 5. The results presented were obtained with the use of two order parameters, namely, (a) $\overline{q_{3\,scaled}}$ and (b) MCG-3. The concentration of methane in the solution ($x^*_{CH_4}$) was equal to 0.042. The size of the clusters of the solid initially inserted into the liquid solution ($N_C^{H_2O}$) is equal to 28.9 in the case of $\overline{q_{3\,scaled}}$ order parameter and 77.6 for MCG-3.

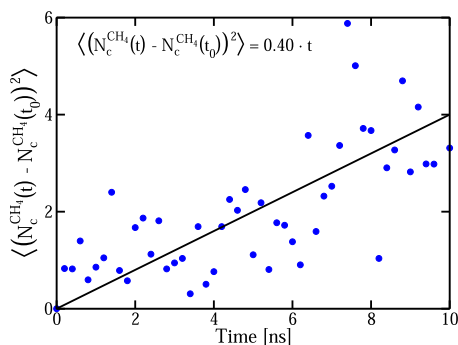**FIG. 9.** $\langle (N_c^{CH_4}(t) - N_c^{CH_4}(t_0))^2 \rangle$ for the critical cluster in a supersaturated solution of methane in water ($S = 4.72$), simulated at 260 K and 400 bars. Results were obtained from the average of ten independent simulations. The size of the cluster of the solid was evaluated using the $\overline{q_{3\,scaled}}$ order parameter (the results for the other order parameters are presented in Sec. S4 of the supplementary material). The attachment rate can be calculated as a half of the slope of the linear fit of the changes of $\langle (N_c^{CH_4}(t) - N_c^{CH_4}(t_0))^2 \rangle$ in time. The fit and its parameters are included in the figure.

TABLE IV. Nucleation rates J [in units of 1/(m^3 s)] obtained from seeding runs in a supersaturated solution of methane in water ($S = 4.72$, 260 K, 400 bars) determined according to Eq. (4), along with values of quantities that were required in calculations. The values of ΔG_c are provided in $k_B T$ units. The attachment rate $f^+_{CH_4}$ is given in s^{-1}. The results obtained with the use of five different order parameters: $\overline{q_3}$, linear combination of $\overline{q_3}$ and $\overline{q_5}$, $\overline{q_{3\,scaled}}$, $\overline{q_{12}}$, and MCG-3 are presented. In calculations, also the values of $\rho_{liq}^{CH_4} = 1.37 \cdot 10^{27}$ 1/m^3, $\rho_{solid}^{CH_4} = 4.6 \cdot 10^{27}$ 1/m^3, and $\Delta\mu^*_{nucleation}/k_B T = 3.97$ were used.[51] For comparison, the nucleation rate obtained from brute force (BF) runs is also included. Additionally, interfacial free energies γ (in mJ/m^2) obtained from seeding are provided (see Sec. III E).

	$\overline{q_3}$	$\overline{q_3}/\overline{q_5}$	MCG-3	$\overline{q_{12}}$	$\overline{q_{3\,scaled}}$	BF
$N_c^{H_2O}$	115	85	78	33	29	
$N_c^{CH_4}$	20	15	14	6	5	
Z	0.102	0.119	0.125	0.190	0.205	
ΔG_c	39.8	29.4	26.8	11.5	10.0	
$f^+_{CH_4}$	$1.2 \cdot 10^9$	$9.0 \cdot 10^8$	$1.1 \cdot 10^9$	$5.6 \cdot 10^8$	$2.0 \cdot 10^8$	
J	$8 \cdot 10^{17}$	$2 \cdot 10^{22}$	$4 \cdot 10^{23}$	$1 \cdot 10^{30}$	$3 \cdot 10^{30}$	$2.5(8) \cdot 10^{30}$
γ	33.2	30.0	29.1	22.0	20.9	

paper of Barnes et al.,[45] where they were able to observe nucleation in brute force runs.

The reader may be surprised by the enormous differences (see Table IV) in the sizes of the critical cluster and in nucleation rates between different reasonable order parameters. This is even more so, taking into account that all these orders parameters are describing the same physical situation. Differences arise from the way that different order parameters see the same physical cluster. However, it should be reminded that CNT (and therefore seeding) works properly only when the order parameter provides a correct estimate of the radius at the surface of tension of the cluster. Different order parameters provide different sizes of the cluster and different estimates

of this radius. The reason why $\overline{q_{3\,scaled}}$ and $\overline{q_{12}}$ are working well is because they provide a good estimate of the radius of the cluster at the surface of tension. We refer the reader to a recent paper[98] where this issue was discussed in detail and also recommend the reading of the original work of Gibbs where this was already pointed out.[94,97]

It is worth to mention here that by assuming a perfect crystalline structure for the critical nucleus, we may be forcing the system to take a higher free energy pathway relative to the one provided by less ordered (i.e., more amorphous) structures (as consistently seen in brute force simulations). However, the impact of this approximation is rather small as the size of the critical nucleus obtained with the use of seeding technique (i.e., $N_c^{H_2O} = 29$ using
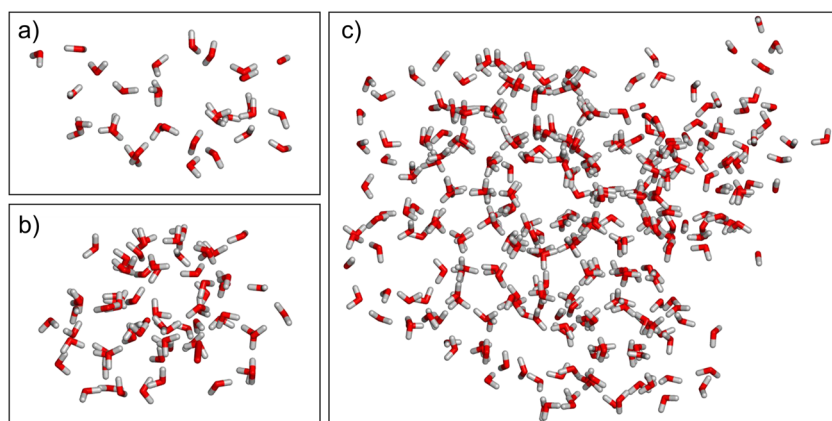
FIG. 10. Snapshots of the cluster of the methane hydrate that nucleated in one of the brute force simulations at $S = 4.72$, shown at different stages of growth: (a) $N^{H_2O} = 32$ (around critical size), (b) $N^{H_2O} = 71$ (post-critical), and (c) $N^{H_2O} = 361$ (post-critical). Molecules of water were assigned as solid with the use of the $\overline{q_{3\,scaled}}$ order parameter. Here, only molecules of water in the cluster are shown (oxygen atoms are shown in red, while hydrogen atoms are shown in white).

the $\overline{q_{3\,scaled}}$ order parameter) is very close to the one obtained from our brute force runs using the MFPT method (i.e., $N_c^{H_2O} = 26$ using the $\overline{q_{3\,scaled}}$ order parameter). In brute force runs, the cluster is not forced to be crystalline, but its critical size is quite similar to the one obtained by inserting a crystalline one into the solution. In Fig. 10, we show the snapshots of the cluster that nucleated in one of the brute force simulations at $S = 4.72$ at different stages of the growth. Figure 10 shows that for the cluster of such a small size, it is difficult to determine whether it is crystalline or amorphous. Additionally, Arjun and Bolhuis[50] have shown recently that both the free energy barrier and the size of the critical nucleus do not differ much when crystalline and amorphous clusters are considered, which further supports our conclusion. Note that whereas in a crystalline cluster, the ratio of large to small cages is three, in an amorphous cluster, this ratio is smaller.

The choice of $\overline{q_{3\,scaled}}$ as the correct order parameter to be used in CNT is further confirmed by using the size of the critical cluster at $S = 4.72$ obtained from brute force simulations (MFPT) and CNT [Eq. (4)] to obtain a predicted nucleation rate of $8 \cdot 10^{30}/(m^3 \, s)$. This value is of the same order of magnitude as the one obtained from a method such as brute force [i.e., $2.5(8) \cdot 10^{30}/(m^3 \, s)$] that does not depend on the choice of the order parameter. All these arguments confirm that $\overline{q_{3\,scaled}}$ works well for the estimation of the size of the critical cluster for seeding and that the assumption of the crystallinity of the cluster does not affect much the nucleation rate.

In previous work,[15] we estimated that a free energy barrier of $13 \, k_B T$ is necessary to obtain the nucleation of ice in brute force simulations when using TIP4P/ICE. The barrier found here is similar. The reason why it is possible to nucleate the hydrate in brute force simulations, whereas it is not possible for ice, is that such a small free energy barrier can be achieved in the case of the hydrate at 260 K (using a highly supersaturated solution), whereas in the case of ice, one needs to go to temperatures around 210 K, where kinetics is terribly slow. In short, $\Delta\mu_{nucleation}$ depends only on T in the case of ice nucleation, whereas in the case of the hydrate, it depends on T and also on the concentration of methane. It is possible to increase x_{CH_4}, which in turn increases $\Delta\mu_{nucleation}$ dramatically, even at high temperatures, making the nucleation process possible.

As mentioned before, the advantage of the $\overline{q_{3\,scaled}}$ order parameter is that the value of $\overline{q_{3\,scaled}^{cut}}$ is located far away from the region

of interfacial water molecules. Because of that, the number of interfacial molecules of water that are mislabeled as solid is significantly lower than in the case of $\overline{q_3}$ and linear combination of $\overline{q_3}$ and $\overline{q_5}$ order parameters. Note, however, that the initial size of the cluster of the solid obtained with the use of $\overline{q_{3\,scaled}^{cut}}$ amounts to 40 out of 46 molecules of water actually present in the solid phase. Because of that, the final size of the cluster of the solid obtained using $\overline{q_{3\,scaled}^{cut}}$ is obtained by using a scaling factor of 46/40 of 46/40, which increments its size by fifteen per cent. The value of N_c obtained by the use of the $\overline{q_{12}}$ order parameter is close to the one obtained with $\overline{q_{3\,scaled}}$.

When it comes to the MCG-3 order parameter, it gives the value of the size of the critical nucleus close to the one obtained with the linear combination of $\overline{q_3}$ and $\overline{q_5}$ order parameters. As can be seen in Table IV, the nucleation rate obtained by the means of seeding using this parameter is not consistent with the result obtained by brute force simulations.

D. Estimation of the nucleation rate at $S = 1$

In Sec. III A we have shown that the $\overline{q_{3\,scaled}}$ and $\overline{q_{12}}$ order parameters give the best results when it comes to the estimation of the nucleation rate using seeding. We will now use these parameters to find the size of the critical nucleus of the methane hydrate in a system where the concentration of methane is equal to its solubility at 260 K and 400 bars. In order to do that, we once again used seeding—we carried out multiple simulations of the liquid solution of methane in water, which was in contact with the methane gas by a planar interface, into which the spherical clusters of the hydrate of different sizes (radii in the range of 1.8–2.0 nm) were inserted. A two-phase gas–liquid system containing around 11 800 molecules of water and around 2800 molecules of methane (in both gas and liquid phases) was prepared and equilibrated at 260 K and 400 bars in the Np_zT ensemble (the planar gas–liquid interfaces were perpendicular to the z axis of the simulation box) for 100 ns. Spherical seeds of different sizes were then cut out from the solid and inserted into the two phase gas–liquid system (the seeds were placed in the center of the liquid phase), while the overlapping molecules from the original two-phase system were removed from the simulation box. The resulting systems contained around 11 000 molecules of water and around 3000 molecules of methane, and their sizes were about $7.2 \times 7.2 \times 10.7 \, nm^3$ (the thicknesses of the liquid and gas phases
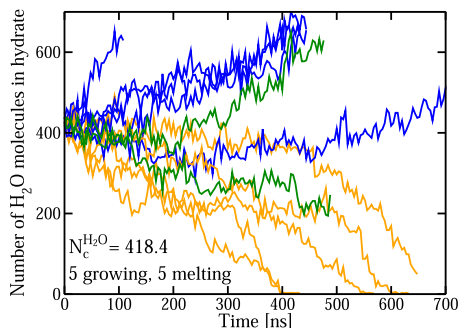
FIG. 11. Changes in time of the size of the largest cluster of a methane hydrate (as a number of water molecules in the cluster) obtained for seeding runs (260 K, 400 bars) in a solution of methane in water, under experimental conditions (i.e., $S = 1$), for a seed size, which is critical. The number of systems in which the cluster of the solid was either growing (blue lines) or melting (orange lines), as well as the size of the critical cluster, is specified. Additionally, results obtained with seeds in which five molecules of methane were removed from the small cages of the hydrate (green lines) are presented. All the results were obtained with the use of the $\overline{q_{3\,scaled}}$ order parameter.

TABLE V. Nucleation rates J in seeding runs in a solution of methane in water (260 K, 400 bars) in which the concentration of methane was equal to the equilibrium solubility under the studied conditions of temperature and pressure (i.e., $S = 1$), determined according to Eq. (4), along with values of quantities that were required in calculations. The values of the error of J were estimated based on the estimated errors of $N_c^{CH_4}$ and $\Delta\mu_{nucleation}^{EC}$ and are provided in here as $\log_{10} J$. The values of ΔG_c are provided in $k_B T$ units. The results obtained with the use of the $\overline{q_{3\,scaled}}$ and $\overline{q_{12}}$ order parameters are presented. In the calculations, also the values of $\rho_{liq}^{CH_4} = 3.03 \cdot 10^{26}$ 1/m^3, $\rho_{solid}^{CH_4} = 4.6 \cdot 10^{27}$ 1/m^3, and $\Delta\mu_{nucleation}^{EC}/k_B T = 2.42$ were used.[51] The superindex EC indicates experimental conditions. Additionally, interfacial free energies γ (in mJ/m^2) obtained from seeding are provided (see Sec. III E).

	$\overline{q_{3\,scaled}}$	$\overline{q_{12}}$	Recommended
$N_C^{H_2O}$	418(6)	478(12)	
$N_C^{CH_4}$	73(1)	83(2)	
Z	0.042	0.039	
ΔG	88.0	100.7	95(6)
$f_{CH_4}^+$ (1/s)	$1.1 \cdot 10^9$	$1.4 \cdot 10^9$	
J [1/(m^3 s)]	$8 \cdot 10^{-5}$	$3 \cdot 10^{-10}$	
$\log_{10} J$	$-4(2)$	$-10(2)$	$-7(5)$
γ (mJ/m^2)	31.1	32.5	

were equal to about 7 and 3.7 nm, respectively). The systems were then simulated at 260 K and 400 bars in the Np_zT ensemble for about 400–750 ns.

In Fig. 11, we present the changes in time of the size of the largest cluster in the system in which the probability of melting or growing of the original seed was close to 50%. The attachment rate is calculated in Fig. 12.

The size of the critical cluster was estimated as an average value of the size of the cluster of the solid during the equilibration period in all the runs using the $\overline{q_{3\,scaled}}$ order parameter—it is equal to 418 molecules of water. Using this value (and data presented in Table V and in Fig. 12), we estimate the nucleation rate for the system using Eq. (4), which is equal to $8 \cdot 10^{-5}$/(m^3 s). Using the same approach, we also estimated the value of the nucleation rate using the $\overline{q_{12}}$ order
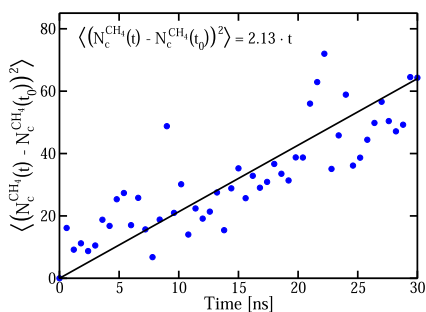

FIG. 12. $\langle (N_c^{CH_4}(t) - N_c^{CH_4}(t_0))^2 \rangle$ vs time for the critical cluster in a solution of methane in water in which the concentration of methane is equal to its equilibrium solubility at 260 K and 400 bars (i.e., $S = 1$). Results were obtained from the average of 10 independent simulations. The size of the cluster of the solid was determined with the use of the $\overline{q_{3\,scaled}}$ order parameter (the results obtained with the use of the $\overline{q_3}$ order parameter are presented in Sec. S5 of the supplementary material). The attachment rate can be calculated as a half of the slope of the linear fit of the changes of $\langle (N_c^{CH_4}(t) - N_c^{CH_4}(t_0))^2 \rangle$ in time—see Table V. The fit and its parameters are included in the figure.

parameter as it was able to reproduce well the brute force nucleation rate for the supersaturated system ($S = 4.72$). The results are included in Table V. The value of J obtained with the $\overline{q_{12}}$ order parameter is equal to $3 \cdot 10^{-10}$/(m^3 s). Since the other order parameters considered in this work were not able to reproduce the nucleation rate obtained for the brute force runs at $S = 4.72$, there is no reason to assume that they would become accurate at S = 1 (in the supplementary material, the value of J at $S = 1$ using the $\overline{q_3}$ order parameter is provided as an example).

Taking into account the two values of the nucleation rate obtained with the $\overline{q_{3\,scaled}}$ and $\overline{q_{12}}$ order parameters at $S = 1$, we conclude that the final recommended value of $\log_{10}$ (J/(m^3 s)) is $-7(5)$. The error of this value is estimated as (2) arising from the statistical uncertainty of a certain order parameter and (3) resulting from the choice of the order parameter (considering only the ones that were able to correctly describe the value of the nucleation rate at S = 4.72).

In Table V, we show that the free energy barrier of nucleation estimated for our system at $S = 1$ (at 260 K and 400 bars) is around 95(6) (in $k_B T$ units). At 260 K and 500 bars, using the same model as in this work, Arjun and Bolhuis[50] found a free energy barrier of 84(7) (in $k_B T$ units). These results are fully in line with ours, considering that at 500 bars, the system has around 2 K of additional supercooling (experimentally, the T_3 temperature increases ~2 K when moving from 400 to 500 bars), and thus, the free energy barrier at 500 bars should be somewhat lower and the nucleation rate should be somewhat larger.

As mentioned in Sec. II, in our simulations, we assumed the full occupancy of the cages in the hydrate. However, in experiments, large cages ($5^{12}6^2$) are almost fully occupied, but the occupancy of the small cages (5^{12}) is only around 85%.[125–128] Moreover, the level of occupancy seen experimentally increases over time (sometimes over a period of weeks),[129] which would imply that in an early stage of the nucleation, the nucleus may have the occupancy lower than

95%. This suggests that the nucleus that is formed in brute force simulation will not consist of fully occupied cages and may not be entirely crystalline.

In order to examine the influence of the occupancy of the cages in the seed inserted into the solution of methane in seeding, we carried out two additional simulations for the seed of critical size from which we removed five molecules of CH_4 from the small cages of the hydrate (5^{12}) to mimic a 94% occupancy. The results are presented in Fig. 11 as green lines. As can be seen, in one of the trajectories, the hydrate cluster grows, and in the other one, it melts. Although, of course, many more trajectories would be needed to determine with accuracy the size of the critical cluster at this lower occupancy, our results indicate that the size of the critical cluster will not be modified by a large amount when reducing the occupancy of the cages from the full occupancy to the experimental value.

It is worth noting that in our estimation of the nucleation rate in the solution at $S = 1$, we assume that the $\overline{q_{3scaled}}$ and $\overline{q_{12}}$ order parameters work in this case and in the case of the supersaturated solution ($S = 4.72$). Since the nucleation rate at $S = 1$ is so low, it is not possible to compare the value obtained using seeding to brute force runs, as we did for $S = 4.72$. Another possibility to check whether our assumption is justified would be to repeat the analysis that we performed for $S = 4.72$ for a solution with a lower supersaturation. However, as can be seen in Fig. 5(a), the time required to observe even a few nucleation events at $S = 4.72$ is already long, and it would be even longer for lower supersaturation. The nucleation rates for lower supersaturations could be therefore obtained rigorously only by using rare event techniques [Transition Path Sampling (TPS), FFS, and US]. As previously mentioned, our seeding estimates at $S = 1$ and 400 bars are fully consistent with the recent calculations by Arjun and Bolhuis[50] at 500 bars by using one of these methods. As found in the previous work,[68] in the particular case of ice nucleation (using mW water model), order parameters that describe well the nucleation rate of brute force simulations were also successful in the estimation of the nucleation rates from seeding under moderate supercooling.

E. Interfacial free energy between the hydrate and the aqueous solution

Let us finish by presenting a brief discussion about the value of the interfacial free energy (γ) between the hydrate and the aqueous solution. From our previous studies with seeding, we know that the value of γ for a fluid–solid interface changes with the radius of curvature of the solid cluster.[130] Thus, the capillarity approximation (i.e., the assumption that the value of γ can be taken from its value of the planar interface) is not a good approximation.[130,131] We have found that this is a quite general conclusion, valid for HS, LJ, and ice Ih–water interfaces.[130]

It seems interesting to analyze this issue in more detail now for the hydrate–water interface. At 260 K and 400 bars, we have found in this work two critical clusters: one obtained when the concentration of methane was given by the solubility of the gas in the aqueous phase via a planar interface (i.e., experimental conditions, $x^0_{CH_4}$) and the other one for a supersaturated solution having a concentration 4.7 times higher (cyan points in Fig. 13). Both of these clusters differ in size (radius, R), and hence, their respective values of γ will be also different.
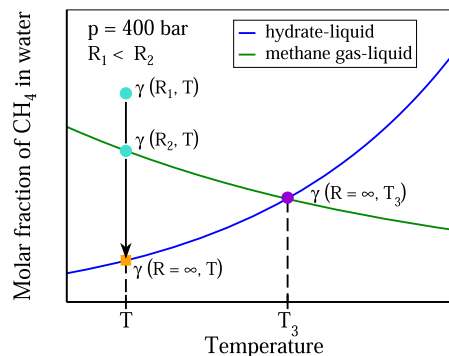

FIG. 13. Schematic depiction of a method of estimating the interfacial free energy between the methane hydrate and aqueous solution of methane in water for a planar solid–liquid interface. At certain p and T, more than one critical cluster can be found for a two component methane–water system depending on the concentration of methane in a solution (cyan points). These clusters differ in terms of their size, and therefore, the values of γ will also be different for each of them. Knowing the relation between the values of γ and the radii of the critical clusters, the value of γ for a planar interface ($R = \infty$) can be estimated (orange square).

Note that when moving along the isobar $T = 260$ K, one can arrive at the concentration of methane equal to the solubility from the solid phase for a planar interface ($R = \infty$, orange square in Fig. 13). By knowing the relation between the radius of the critical cluster and γ, it is possible to estimate the value of the surface free energy for the planar interface.

The value of γ from the seeding runs can be obtained from CNT by using the expression

$$\gamma = \left(\frac{3 \cdot \left(\rho^{CH_4}_{solid}\right)^2 \cdot \left(|\Delta\mu_{nucleation}|\right)^3 \cdot N^{CH_4}_c}{32\pi} \right)^{1/3}. \quad (20)$$

Values of γ are reported in Tables IV and V. The value of the radius of the cluster can be estimated easily by using the number of molecules of methane in the critical cluster and the number density of methane in the bulk hydrate phase using the expression

$$R = \sqrt[3]{\frac{3 \cdot N^{CH_4}_c}{4\pi \cdot \rho^{CH_4}_{solid}}}. \quad (21)$$

In Fig. 14, the values of γ vs $1/R$ for two critical clusters that we found for systems at 260 K and 400 bars are plotted (cyan points).

As can be seen, γ increases with the radius of the cluster, and our calculations suggest a value of around 38 mJ/m^2 for the planar interface (orange square in Fig. 14). Note that both the concentration of methane and the radius of the cluster are different in the two points represented in Fig. 14—it is more clearly depicted in Fig. 13. We cannot state if the change in γ is due to the change of R or the change in the concentration of methane since both variables are coupled for the critical cluster (the same happened when plotting the value of γ as a function of $1/R$ along an isobar when considering the case of the ice Ih–water interface, as in this case, both the change in the radius and the change in T are coupled). For the ice Ih–water interface and the basal crystallographic plane, a value of about 29–31 mJ/m^2 at 400 bars can be roughly estimated based on
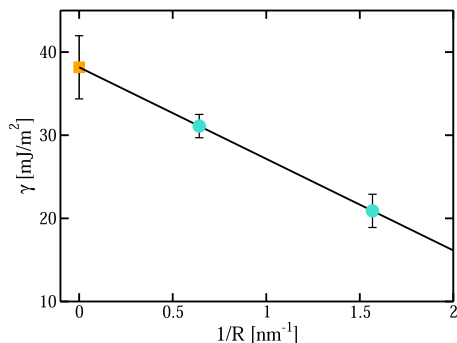
FIG. 14. Values of the interfacial free energy between the hydrate and the aqueous phase as found in this work from seeding (using the $\overline{q}_{3\,scaled}$ order parameter) as a function of the inverse of the radius of the cluster (cyan points). The values are fitted to a linear function (black solid line), which indicates the value of the interfacial free energy of a planar interface equal to 38 mJ/m² (orange square). Here, the estimated values of the error of γ are provided as error bars. In all cases, the systems were simulated at 260 K and 400 bars.

the previous work.[52] Thus, the results of this work seem to suggest a higher value of γ for the planar hydrate–water interface as compared to the planar ice Ih–water interface when compared at the same temperature and pressure. It is worth to point out here that in the case of the ice–water system, there is only one temperature at which the two phases are in equilibrium under a certain pressure, while in the case of the hydrate–liquid system, the temperature of coexistence changes depending on the concentration of methane. Therefore, for the hydrate–liquid system, one can have multiple values of γ for the
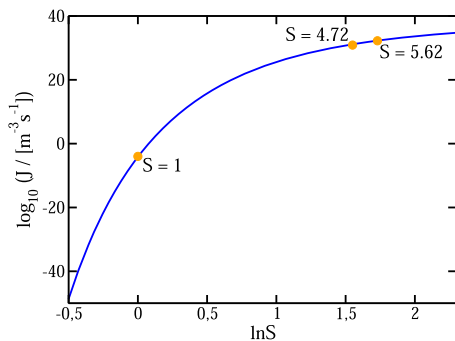

FIG. 15. Nucleation rate (at 260 K and 400 bars) as a function of the natural logarithm of the supersaturation of the solution of methane in water, as estimated in this work using CNT theory [i.e., Eqs. (4) and (5)]. The following expressions were used when implementing the theory: $|\Delta \mu_{nucleation}/(k_B T)| = 2.42 + \ln(S)$ (i.e., including the rigorous value of the driving force for $S = 1$, neglecting changes in the chemical potential of water with S and describing the chemical potential of methane as in an ideal solution) and $\gamma/(mJ/m^2) = 31.1 - 6.573 \ln(S)$ (as obtained from the seeding runs of this work for $S = 1$ and $S = 4.72$ when analyzed with the $\overline{q}_{3\,scaled}$ order parameter). We assumed that the attachment rate is constant (i.e., $f^+_{CH_4}/s = 1 \cdot 10^9$) and obtained $N_c^{CH_4}$ from the standard expression of CNT [see Eq. (3) of Ref. 68]. Number density of methane in the fluid phase is obtained by multiplying its value at $S = 1$ by S, and the number density of methane in the solid phase does not depend on S, and it was obtained from simulations of the hydrate at 260 K and 400 bars (see the caption of Table V).

planar interface (under a certain pressure) while moving along the solid–liquid coexistence line (blue solid line in Fig. 13).

The value found here for the planar interface for the methane hydrate seems to be higher than the value found by Anderson *et al.*,[132] which is equal to 32 mJ/m² and the value of about 29–30 mJ/m² found recently for carbon dioxide hydrate[133,134] at T_3 and 400 bars. It would be interesting to determine in the future the value of γ of the methane hydrate by using mold integration[135] for the models of water and methane used in this work (as it has been done recently for the carbon dioxide hydrate[133,134]) to confirm the larger value of γ suggested by the results of this work.

Let us finish by estimating the nucleation rate of the formation of the methane hydrate at 260 K and 400 bars as a function of the supersaturation of the solution, S. In order to do that, we shall use the expressions of CNT along with the input obtained from the seeding runs of this work. The result is shown in Fig. 15. As can be seen, the nucleation rate decreases rapidly with the concentration of the methane at lower supersaturations and increases slowly at high supersaturations. It is also clear that at a certain pressure and temperature, the nucleation rate of methane hydrate can be either enormous or practically negligible depending on the concentration of methane in the solution.

IV. CONCLUSIONS

In this work, we have employed seeding to estimate the homogeneous nucleation rate of the methane hydrate at 400 bars for a supercooling of 35 K. Depending on the order parameter, we obtain quite different values of nucleation rates. To decide which one could be more reliable, we performed brute force simulations in a supersaturated solution of methane in water where nucleation can be obtained in long but still feasible computer times. In this way, we obtained the value of the nucleation rate under the same conditions without any ambiguity. After that, we implemented seeding runs and checked which one among different possible order parameters was able to provide estimates consistent with the results from the brute force runs.

It turns out that common order parameters[100,118] were not able to predict correctly the value of J found from brute force runs. In general, these order parameters provide values of J much lower than the correct value. It follows from that that these order parameters exaggerate the size of the critical cluster and, therefore, overestimate the radius of the solid cluster at the surface of tension, which is the one that enters in CNT. We have shown that only two of the considered order parameters ($\overline{q}_{3\,scaled}$ and $\overline{q}_{12}$) were able to provide predictions of J for the supersaturated solution in good agreement with the exact results.

Subsequently, we implemented the technique of seeding under experimental conditions in a system having two phases (methane and water) in equilibrium. We determined the size of the critical cluster using the order parameters that were successful for the supersaturated solution and determined the value of J, which was found to be of the order of $10^{-7}/(m^3 \text{ s})$. This value means that for a sample having 10 cm³ in the aqueous phase, it would take 10^{12} s to homogeneously nucleate (i.e., 32 thousands years) or 320 years for a sample having 1 l of the aqueous phase. It is clear that the homogeneous nucleation rate is rather small. Why does it happen in real experiments when having the gas in contact with the water with a planar

interface? It has been shown quite recently by Bian *et al.*[106] (see Fig. 4 of their paper) that even for a supercooling of around 5 K, the nucleation occurs in less than twenty minutes (this time is usually called the induction time in experiments). How to solve the contradiction between our predictions and experiments? The answer is simple. In experiments, the formation of the hydrate must occur via heterogeneous nucleation.[24,106,136] However, simulations such as those presented in this work allow us to determine the value of the homogeneous nucleation rate. In the future, it will be of interest to study the heterogeneous route[103,137,138] at a molecular level.

It is interesting to discuss briefly whether ice Ih could nucleate first under the experimental conditions (i.e., 260 K and 400 bars). The answer is negative. The melting point at 400 bars of ice Ih is around 270 K in experiments and 267 K for the TIP4P/ICE model.[139] The system at 260 K and 400 bars is only at 7 K of supercooling with respect to ice formation. We found in previous work[15] that the nucleation rate of the ice formation at 1 bar is as low as $10^{-173}/(m^3 \, s)$ even for a higher supercooling (15 K). Therefore, just looking at the equilibrium points at this pressure (267 K for ice–water equilibrium and 295 K for the hydrate–water equilibrium), one can conclude that the nucleation of ice is impossible because at any temperature, the supercooling for the hydrate formation is 28 K higher than the supercooling for the ice formation. Since J goes to zero as one reaches the equilibrium temperature, the formation of ice is impossible. One can either have the metastable mixture of water and methane or the stable mixture of the hydrate and the fluid.

A related but different question is as follows. How does the nucleation rate of ice compare to that of the hydrate when they are at the same supercooling? In this case, we should compare at 400 bars the nucleation rate for the hydrate formation at 260 K to that of the ice formation at 232 K (i.e., with 35 K of supercooling in both cases). In previous work, we estimated the nucleation rate of ice[139] at 400 bars and 232 K to be around $J = 10^5/(m^3 \, s)$. Thus, it seems that the nucleation of ice is faster than that of the hydrate when compared at the same supercooling. We have shown recently that the driving force for nucleation ($\Delta \mu_{nucleation}$) when computed per molecule of water is larger for the hydrate than for ice formation. All other things being equal would suggest higher nucleation rates for the hydrate. Since we found the opposite, that strongly suggests that the value of the interfacial free energy for the hydrate–water interface is higher than that of the ice Ih–water interface at 400 bars. Some indirect evidence of this finding was found in this work.

Let us finally state that at 400 bars, any hydrate formation at temperatures significantly above 260 K found in experiments must be due to heterogeneous nucleation. We hope that the results of this work can be useful for other groups trying to obtain the nucleation rate under the same conditions using more elaborate methodologies as transition path sampling[53,59] or forward flux sampling.[99]

SUPPLEMENTARY MATERIAL

See the supplementary material for the data regarding the calculation of the nucleation rate of the hydrate in a supersaturated system from the brute force runs using the $\overline{q_3}$ order parameter and additional results for the seeding in a supersaturated solution and for the seeding in a two-phase gas–liquid system.

AUTHOR DECLARATIONS

Conflict of Interest

The authors have no conflicts to disclose.

Author Contributions

J. Grabowska: Conceptualization (equal); Data curation (lead); Formal analysis (lead); Investigation (equal); Writing – original draft (equal); Writing – review & editing (equal). **S. Blazquez**: Conceptualization (lead); Data curation (equal); Investigation (equal); Methodology (equal); Supervision (equal); Writing – original draft (equal); Writing – review & editing (equal). **E. Sanz**: Conceptualization (equal); Data curation (equal); Investigation (equal); Methodology (equal); Writing – review & editing (equal). **E. G. Noya**: Conceptualization (equal); Formal analysis (equal); Methodology (equal); Writing – review & editing (equal). **I. M. Zeron**: Formal analysis (equal); Investigation (equal); Methodology (equal); Writing – review & editing (equal). **J. Algaba**: Investigation (equal); Methodology (equal); Writing – review & editing (equal). **J. M. Miguez**: Investigation (equal); Methodology (equal); Writing – review & editing (equal). **F. J. Blas**: Conceptualization (equal); Investigation (equal); Methodology (equal); Writing – review & editing (equal). **C. Vega**: Conceptualization (lead); Investigation (lead); Methodology (equal); Supervision (equal); Writing – original draft (equal); Writing – review & editing (equal).

DATA AVAILABILITY

The data that support the findings of this study are available within the article and its supplementary material.

REFERENCES

[1] E. D. Sloan and C. A. Koh, *Clathrate Hydrates of Natural Gases*, 3rd ed. (CRC Press, 2007).

[2] V. Chihaia, S. Adams, and W. F. Kuhs, Chem. Phys. **317**, 208 (2005).

[3] P. G. Debenedetti, *Metastable Liquids: Concepts and Principles* (Princeton University Press, 1996).

[4] H. R. Pruppacher, J. Atmos. Sci. **52**, 1924 (1995).

[5] C. A. Stan, G. F. Schneider, S. S. Shevkoplyas, M. Hashimoto, M. Ibanescu, B. J. Wiley, and G. M. Whitesides, Lab Chip **9**, 2293 (2009).

[6] P. Taborek, Phys. Rev. B **32**, 5902 (1985).

[7] P. J. DeMott and D. C. Rogers, J. Atmos. Sci. **47**, 1056 (1990).

[8] P. Stöckel, I. M. Weidinger, H. Baumgärtel, and T. Leisner, J. Phys. Chem. A **109**, 2540 (2005).

[9] B. Krämer, O. Hübner, H. Vortisch, L. Wöste, T. Leisner, M. Schwell, E. Rühl, and H. Baumgärtel, J. Chem. Phys. **111**, 6521 (1999).

[10] D. Duft and T. Leisner, Atmos. Chem. Phys. **4**, 1997 (2004).

[11] H. Laksmono, T. A. McQueen, J. A. Sellberg, N. D. Loh, C. Huang, D. Schlesinger, R. G. Sierra, C. Y. Hampton, D. Nordlund, M. Beye, A. V. Martin, A. Barty, M. M. Seibert, M. Messerschmidt, G. J. Williams, S. Boutet, K. Amann-Winkel, T. Loerting, L. G. M. Pettersson, M. J. Bogan, and A. Nilsson, J. Phys. Chem. Lett. **6**, 2826 (2015).

[12] A. Manka, H. Pathak, S. Tanimura, J. Wölk, R. Strey, and B. E. Wyslouzil, Phys. Chem. Chem. Phys. **14**, 4505 (2012).

[13] D. E. Hagen, R. J. Anderson, and J. L. Kassner, J. Atmos. Sci. **38**, 1236 (1981).

[14] E. Sanz, C. Vega, J. R. Espinosa, R. Caballero-Bernal, J. L. F. Abascal, and C. Valeriani, J. Am. Chem. Soc. **135**, 15008 (2013).

[15] J. R. Espinosa, E. Sanz, C. Valeriani, and C. Vega, J. Chem. Phys. **141**, 18C529 (2014).

[16] T. Li, D. Donadio, G. Russo, and G. Galli, Phys. Chem. Chem. Phys. **13**, 19807 (2011).

[17] A. Haji-Akbari and P. G. Debenedetti, Proc. Natl. Acad. Sci. U. S. A. **112**, 10582 (2015).

[18] A. Haji-Akbari, R. S. DeFever, S. Sarupria, and P. G. Debenedetti, Phys. Chem. Chem. Phys. **16**, 25916 (2014).

[19] J. Russo, F. Romano, and H. Tanaka, Nat. Mater. **13**, 733 (2014).

[20] B. Cheng, C. Dellago, and M. Ceriotti, Phys. Chem. Chem. Phys. **20**, 28732 (2018).

[21] H. Niu, Y. I. Yang, and M. Parrinello, Phys. Rev. Lett. **122**, 245501 (2019).

[22] J. R. Espinosa, C. Navarro, E. Sanz, C. Valeriani, and C. Vega, J. Chem. Phys. **145**, 211922 (2016).

[23] L. Ickes, A. Welti, C. Hoose, and U. Lohmann, Phys. Chem. Chem. Phys. **17**, 5514 (2015).

[24] P. Warrier, M. N. Khan, V. Srivastava, C. M. Maupin, and C. A. Koh, J. Chem. Phys. **145**, 211705 (2016).

[25] W. Ke, T. M. Svartaas, and D. Chen, J. Nat. Gas Sci. Eng. **61**, 169 (2019).

[26] H. K. Abay and T. M. Svartaas, Energy Fuels **25**, 42 (2011).

[27] J. M. Herri, J. S. Pic, F. Gruy, and M. Cournil, AIChE J. **45**, 590 (1999).

[28] K. Lekvam and P. Ruoff, J. Am. Chem. Soc. **115**, 8565 (1993).

[29] S. Devarakonda, A. Groysman, and A. S. Myerson, J. Cryst. Growth **204**, 525 (1999).

[30] S. Takeya, A. Hori, T. Hondoh, and T. Uchida, J. Phys. Chem. B **104**, 4164 (2000).

[31] L. Jensen, K. Thomsen, and N. von Solms, Chem. Eng. Sci. **63**, 3069 (2008).

[32] N. Maeda, Fuel **223**, 286 (2018).

[33] N. Maeda and X.-d. Shen, Fuel **253**, 1597 (2019).

[34] S. Sarupria and P. G. Debenedetti, J. Phys. Chem. Lett. **3**, 2942 (2012).

[35] B. C. Knott, V. Molinero, M. F. Doherty, and B. Peters, J. Am. Chem. Soc. **134**, 19544 (2012).

[36] S. Liang and P. G. Kusalik, J. Phys. Chem. B **117**, 1403 (2013).

[37] A. Arjun, T. A. Berendsen, and P. G. Bolhuis, Proc. Natl. Acad. Sci. U. S. A. **116**, 19305 (2019).

[38] A. Arjun and P. G. Bolhuis, J. Phys. Chem. B **124**, 8099 (2020).

[39] A. Arjun and P. G. Bolhuis, J. Comput. Phys. **154**, 164507 (2021).

[40] M. R. Walsh, C. A. Koh, E. D. Sloan, A. K. Sum, and D. T. Wu, Science **326**, 1095 (2009).

[41] L. A. Báez and P. Clancy, Ann. N. Y. Acad. Sci. **715**, 177 (1994).

[42] P. M. Rodger, T. R. Forester, and W. Smith, Fluid Phase Equilib. **116**, 326 (1996).

[43] M. Lauricella, G. Ciccotti, N. J. English, B. Peters, and S. Meloni, J. Phys. Chem. C **121**, 24223 (2017).

[44] Z. Zhang, C.-J. Liu, M. R. Walsh, and G.-J. Guo, Phys. Chem. Chem. Phys. **18**, 15602 (2016).

[45] B. C. Barnes, B. C. Knott, G. T. Beckham, D. T. Wu, and A. K. Sum, J. Phys. Chem. B **118**, 13236 (2014).

[46] D. Yuhara, B. C. Barnes, D. Suh, B. C. Knott, G. T. Beckham, K. Yasuoka, D. T. Wu, and A. K. Sum, Faraday Discuss. **179**, 463 (2015).

[47] Y. Bi and T. Li, J. Phys. Chem. B **118**, 13324 (2014).

[48] M. R. Walsh, G. T. Beckham, C. A. Koh, E. D. Sloan, D. T. Wu, and A. K. Sum, J. Phys. Chem. C **115**, 21241 (2011).

[49] Z. Zhang, N. Wu, C. Liu, X. Hao, Y. Zhang, K. Gao, B. Peng, C. Zheng, W. Tang, and G. Guo, China Geol. **5**, 330 (2022).

[50] A. Arjun and P. G. Bolhuis, J. Chem. Phys. **158**, 044504 (2023).

[51] J. Grabowska, S. Blazquez, E. Sanz, I. M. Zerón, J. Algaba, J. M. Míguez, F. J. Blas, and C. Vega, J. Phys. Chem. B **126**, 8553 (2022).

[52] J. R. Espinosa, A. Zaragoza, P. Rosales-Pelaez, C. Navarro, C. Valeriani, C. Vega, and E. Sanz, Phys. Rev. Lett. **117**, 135702 (2016).

[53] P. G. Bolhuis, D. Chandler, C. Dellago, and P. L. Geissler, Annu. Rev. Phys. Chem. **53**, 291 (2002).

[54] R. J. Allen, P. B. Warren, and P. R. ten Wolde, Phys. Rev. Lett. **94**, 018104 (2005).

[55] G. M. Torrie and J. P. Valleau, Chem. Phys. Lett. **28**, 578 (1974).

[56] G. M. Torrie and J. P. Valleau, J. Comput. Phys. **23**, 187 (1977).

[57] A. Barducci, G. Bussi, and M. Parrinello, Phys. Rev. Lett. **100**, 020603 (2008).

[58] A. Laio and F. L. Gervasio, Rep. Prog. Phys. **71**, 126601 (2008).

[59] C. Dellago, P. G. Bolhuis, F. S. Csajka, and D. Chandler, J. Chem. Phys. **108**, 1964 (1998).

[60] Y. Zhang, L. Zhao, S. Deng, R. Zhao, X. Nie, and Y. Liu, J. Therm. Sci. **28**, 948 (2019).

[61] Y. Lu, L. Yang, Y. Kuang, Y. Song, J. Zhao, and A. K. Sum, Phys. Chem. Chem. Phys. **23**, 27533 (2021).

[62] T. Uchida, K. Yamazaki, and K. Gohara, J. Phys. Chem. C **120**, 26620 (2016).

[63] S. A. Bagherzadeh, S. Alavi, J. Ripmeester, and P. Englezos, J. Chem. Phys. **142**, 214701 (2015).

[64] J. A. Ripmeester and S. Alavi, Curr. Opin. Solid State Mater. Sci. **20**, 344 (2016).

[65] J. L. F. Abascal, E. Sanz, R. García Fernández, and C. Vega, J. Chem. Phys. **122**, 234511 (2005).

[66] B. Guillot and Y. Guissani, J. Chem. Phys. **99**, 8075 (1993).

[67] D. Paschek, J. Chem. Phys. **120**, 6674 (2004).

[68] J. R. Espinosa, C. Vega, C. Valeriani, and E. Sanz, J. Chem. Phys. **144**, 034501 (2016).

[69] X.-M. Bai and M. Li, J. Chem. Phys. **122**, 224510 (2005).

[70] X.-M. Bai and M. Li, J. Chem. Phys. **124**, 124707 (2006).

[71] R. G. Pereyra, I. Szleifer, and M. A. Carignano, J. Chem. Phys. **135**, 034508 (2011).

[72] P. Montero de Hijes, J. R. Espinosa, V. Bianco, E. Sanz, and C. Vega, J. Phys. Chem. C **124**, 8795 (2020).

[73] I. Sanchez-Burgos, E. Sanz, C. Vega, and J. R. Espinosa, Phys. Chem. Chem. Phys. **23**, 19611 (2021).

[74] J. R. Espinosa, C. Vega, C. Valeriani, D. Frenkel, and E. Sanz, Soft Matter **15**, 9625 (2019).

[75] I. Sanchez-Burgos, P. Montero de Hijes, P. Rosales-Pelaez, C. Vega, and E. Sanz, Phys. Rev. E **102**, 062609 (2020).

[76] P. M. Piaggi, J. Weis, A. Z. Panagiotopoulos, P. G. Debenedetti, and R. Car, Proc. Natl. Acad. Sci. U. S. A. **119**, e227294119 (2022).

[77] C. P. Lamas, J. R. Espinosa, M. M. Conde, J. Ramírez, P. Montero de Hijes, E. G. Noya, C. Vega, and E. Sanz, Phys. Chem. Chem. Phys. **23**, 26843 (2021).

[78] N. E. R. Zimmermann, B. Vorselaars, J. R. Espinosa, D. Quigley, W. R. Smith, E. Sanz, C. Vega, and B. Peters, J. Chem. Phys. **148**, 222838 (2018).

[79] J. R. Espinosa, G. D. Soria, J. Ramirez, C. Valeriani, C. Vega, and E. Sanz, J. Phys. Chem. Lett. **8**, 4486 (2017).

[80] M. Volmer and A. Weber, Z. Phys. Chem. **119U**, 277 (1926).

[81] R. Becker and W. Döring, Ann. Phys. **416**, 719 (1935).

[82] K. F. Kelton, *Crystal Nucleation in Liquids and Glasses* (Academic Press, Boston, 1991), Vol. 45.

[83] S. Auer and D. Frenkel, Nature **409**, 1020 (2001).

[84] S. Auer and D. Frenkel, Annu. Rev. Phys. Chem. **55**, 333 (2004).

[85] A. Cacciuto, S. Auer, and D. Frenkel, Nature **428**, 404 (2004).

[86] R. Blaak, S. Auer, D. Frenkel, and H. Lowen, Phys. Rev. Lett. **93**, 068303 (2004).

[87] L. Filion, M. Hermes, R. Ni, and M. Dijkstra, J. Chem. Phys. **133**, 244115 (2010).

[88] P. Virnau and M. Müller, J. Chem. Phys. **120**, 10925 (2004).

[89] A. Reinhardt and J. P. K. Doye, J. Chem. Phys. **136**, 054501 (2012).

[90] Y. Goswami, V. V. Vasisht, D. Frenkel, P. G. Debenedetti, and S. Sastry, J. Chem. Phys. **155**, 194502 (2021).

[91] C. Valeriani, E. Sanz, and D. Frenkel, J. Chem. Phys. **122**, 194501 (2005).

[92] V. Molinero and E. B. Moore, J. Phys. Chem. B **113**, 4008 (2009).

[93] S. Prestipino, J. Chem. Phys. **148**, 124505 (2018).

[94] J. W. Gibbs, Trans. Conn. Acad. **3**, 343 (1877).

[95] S. Kondo, J. Chem. Phys. **25**, 662 (1956).

[96] W. W. Mullins, J. Chem. Phys. **81**, 1436 (1984).

[97] D. Kashchiev, J. Chem. Phys. **153**, 124509 (2020).

[98] P. Montero de Hijes and C. Vega, J. Chem. Phys. **156**, 014505 (2022).

[99] R. J. Allen, C. Valeriani, and P. R. ten Volde, J. Phys.: Condens. Matter. **21**, 463102 (2009).

[100] W. Lechner and C. Dellago, J. Chem. Phys. **129**, 114707 (2008).

[101] S. Auer and D. Frenkel, J. Phys.: Condens. Matter **120**, 3015 (2004).

[102] D. Kashchiev and A. Firoozabadi, J. Cryst. Growth **241**, 220 (2002).

[103] D. Kashchiev and A. Firoozabadi, J. Cryst. Growth **243**, 476 (2002).

[104] P. Servio and P. Englezos, J. Chem. Eng. Data **47**, 87 (2002).

[105] E. M. Freer, M. S. Selim, and E. D. Sloan, Fluid Phase Equilib. **185**, 65 (2001).

[106] H. Bian, L. Ai, J. Y. Y. Heng, G. C. Maitland, and K. Hellgardt, Chem. Eng. J. **452**, 139084 (2023).

[107] J. M. Schicks, ChemTexts **8**, 13 (2022).

[108] D. van der Spoel, E. Lindahl, B. Hess, G. Groenhof, A. E. Mark, and H. J. C. Berendsen, J. Comput. Chem. **26**, 1701 (2005).

[109] B. Hess, C. Kutzner, D. van der Spoel, and E. Lindahl, J. Chem. Theory Comput. **4**, 435 (2008).

[110] M. Parrinello and A. Rahman, J. Appl. Phys. **52**, 7182 (1981).

[111] S. Nosé, Mol. Phys. **52**, 255 (1984).

[112] W. G. Hoover, Phys. Rev. A **31**, 1695 (1985).

[113] B. Hess, H. Bekker, H. J. C. Berendsen, and J. G. E. M. Fraaije, J. Comput. Chem. **18**, 1463 (1997).

[114] B. Hess, J. Chem. Theory Comput. **4**, 116 (2008).

[115] P. E. Brumby, D. Yuhara, D. T. Wu, A. K. Sum, and K. Yasuoka, Fluid Phase Equilib. **413**, 242 (2016).

[116] J. D. Bernal and R. H. Fowler, J. Chem. Phys. **1**, 515 (1933).

[117] V. Buch, P. Sandler, and J. Sadlej, J. Phys. Chem. B **102**, 8641 (1998).

[118] B. C. Barnes, G. T. Beckham, D. T. Wu, and A. K. Sum, J. Chem. Phys. **140**, 164506 (2014).

[119] J. Wedekind, R. Strey, and D. Reguera, J. Chem. Phys. **126**, 134103 (2007).

[120] G. Chkonia, J. Wölk, R. Strey, J. Wedekind, and D. Reguera, J. Chem. Phys. **130**, 064505 (2008).

[121] L. Li, J. Zhong, Y. Yan, J. Zhang, J. Xu, J. S. Francisco, and X. C. Zeng, Proc. Natl. Acad. Sci. U. S. A. **117**, 24701 (2020).

[122] L. C. Jacobson, W. Hujo, and V. Molinero, J. Am. Chem. Soc. **132**, 11806 (2010).

[123] J. Vatamanu and P. G. Kusalik, Phys. Chem. Chem. Phys. **12**, 15065 (2010).

[124] H. Jiang, P. G. Debenedetti, and A. Z. Panagiotopoulos, J. Chem. Phys. **150**, 124502 (2019).

[125] R. Susilo, J. A. Ripmeester, and P. Englezos, Chem. Eng. Sci. **62**, 3930–3939 (2007).

[126] S. Takeya, K. A. Udachin, I. L. Moudrakovski, R. Susilo, and J. A. Ripmeester, J. Am. Chem. Soc. **132**, 524–531 (2010).

[127] W. Cai, X. Huang, and H. Lu, Energies **15**, 485 (2022).

[128] R. W. Henning, A. J. Schultz, V. Thieu, and Y. Halpern, J. Phys. Chem. A **104**, 5066 (2000).

[129] C. Petuya, F. Damay, S. Desplanche, C. Aupetit, and A. Desmedt, Crystals **8**, 145 (2018).

[130] P. Montero de Hijes, J. R. Espinosa, E. Sanz, and C. Vega, J. Chem. Phys. **151**, 144501 (2019).

[131] J. Rowlinson and B. Widom, *Molecular Theory of Capillarity* (Clarendon, Oxford, 1982).

[132] R. Anderson, M. Llamedo, B. Tohidi, and R. W. Burgass, J. Phys. Chem. **107**, 3507 (2003).

[133] J. Algaba, E. Acuña, J. M. Míguez, B. Mendiboure, I. M. Zerón, and F. J. Blas, J. Colloid Interface Sci. **623**, 354 (2022).

[134] I. M. Zerón, J. M. Míguez, B. Mendiboure, J. Algaba, and F. J. Blas, J. Chem. Phys. **157**, 134709 (2022).

[135] J. R. Espinosa, C. Vega, and E. Sanz, J. Chem. Phys. **141**, 134709 (2014).

[136] V. Natarajan, P. R. Bishnoi, and N. Kalogerakis, Chem. Eng. Sci. **49**, 2075 (1994).

[137] G.-J. Guo and P. M. Rodger, J. Phys. Chem. B **117**, 6498 (2013).

[138] L. Boewer, J. Nase, M. Paulus, F. Lehmkühler, S. Tiemeyer, S. Holz, D. Pontoni, and M. Tolan, J. Phys. Chem. C **116**, 8548 (2012).

[139] V. Bianco, P. Montero de Hijes, C. P. Lamas, E. Sanz, and C. Vega, Phys. Rev. Lett. **126**, 015704 (2021).

26 February 2024 09:34:05